

AD-A272 493



2

NAVAL POSTGRADUATE SCHOOL Monterey, California

S DTIC
ELECTE
NOV 05 1993
A **D**



THESIS

Incorporation and Comparative Evaluation
of a Non-convective Cloud Parameterization
Scheme in the Naval Research Laboratory
West Coast Mesoscale Weather
Prediction Model

by

Damacene V. Fernandez

June 1993

Thesis Advisor: Teddy R. Holt

Approved for public release;
distribution is unlimited

93-26685



010

REPORT DOCUMENTATION PAGE				Form Approved OMB No 0704-0188	
1a REPORT SECURITY CLASSIFICATION Unclassified		1b RESTRICTIVE MARKINGS			
2a SECURITY CLASSIFICATION AUTHORITY		3 DISTRIBUTION / AVAILABILITY OF REPORT Approved for public release; distribution is unlimited			
2b DECLASSIFICATION / DOWNGRADING SCHEDULE		4 PERFORMING ORGANIZATION REPORT NUMBER(S)			
4 PERFORMING ORGANIZATION REPORT NUMBER(S)		5 MONITORING ORGANIZATION REPORT NUMBER(S)			
6a NAME OF PERFORMING ORGANIZATION Naval Postgraduate School		6b OFFICE SYMBOL (if applicable) 35	7a NAME OF MONITORING ORGANIZATION Naval Postgraduate School		
6c ADDRESS (City, State, and ZIP Code) Monterey, CA 93943-5000		7b ADDRESS (City, State, and ZIP Code) Monterey, CA 93943-5000			
8a NAME OF FUNDING / SPONSORING ORGANIZATION		8b OFFICE SYMBOL (if applicable)	9 PROCUREMENT INSTRUMENT IDENTIFICATION NUMBER		
8c ADDRESS (City, State, and ZIP Code)		10 SOURCE OF FUNDING NUMBERS			
		PROGRAM ELEMENT NO	PROJECT NO	TASK NO	WORK UNIT ACCESSION NO
11 TITLE (Include Security Classification) INCORPORATION AND COMPARATIVE EVALUATION OF A NON-CONVECTIVE CLOUD PARAMETERIZATION SCHEME IN THE NAVAL RESEARCH LABORATORY WEST COAST MESOSCALE WEATHER PREDICTION MODEL					
12 PERSONAL AUTHOR(S) Damacene V. Ferandez					
13a TYPE OF REPORT Master's Thesis		13b TIME COVERED FROM _____ TO _____	14 DATE OF REPORT (Year, Month, Day) 1993 June		15 PAGE COUNT 84
16 SUPPLEMENTARY NOTATION The views expressed in this thesis are those of the author and do not reflect the official policy or position of the Department of Defense or the U.S. Government.					
17 COSATI CODES		18 SUBJECT TERMS (Continue on reverse if necessary and identify by block number)			
FIELD	GROUP	SUB-GROUP			
19 ABSTRACT (Continue on reverse if necessary and identify by block number) This study describes the incorporation of the Sundqvist et al. (1989) explicit non-convective cloud liquid water scheme into the Naval Research Laboratory (NRL) limited area dynamical weather prediction model. Comparisons were made between model runs with the non-convective cloud water scheme and those without the scheme to evaluate mesoscale wind pattern, longwave radiation, temperature, and cloud simulations over the U.S. West Coast for the time period 0000 UTC 02 May 1990 to 1200 UTC 03 May 1990. The most significant improvement in the updated model was the more physically realistic horizontal and vertical non-convective cloud structures produced by the cloud liquid water fields.					
20 DISTRIBUTION / AVAILABILITY OF ABSTRACT <input checked="" type="checkbox"/> UNCLASSIFIED/UNLIMITED <input type="checkbox"/> SAME AS RPT <input type="checkbox"/> DTIC USERS			21 ABSTRACT SECURITY CLASSIFICATION Unclassified		
22a NAME OF RESPONSIBLE INDIVIDUAL T.R. Holt		22b TELEPHONE (Include Area Code) (408) 656-2861		22c OFFICE SYMBOL MR/Ht	

Approved for public release; distribution is unlimited.

Incorporation and Comparative Evaluation of a
Non-Convective Cloud Parameterization Scheme
in the Naval Research Laboratory West Coast
Mesoscale Weather Prediction Model

by

Damacene V. Ferandez
Lieutenant Commander, United States Navy
B.S., U.S. Naval Academy, 1981

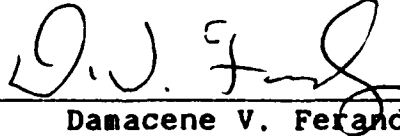
Submitted in partial fulfillment of the
requirements for the degree of

MASTER OF SCIENCE IN METEOROLOGY
AND PHYSICAL OCEANOGRAPHY

from the

NAVAL POSTGRADUATE SCHOOL
June 1993

Author:

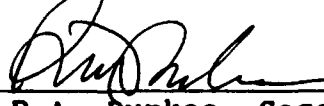


Damacene V. Ferandez

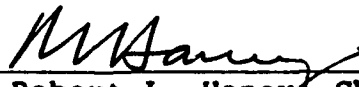
Approved by:



T.R. Holt, Thesis Advisor



P.A. Durkee, Second Reader



Robert L. Haney, Chairman,
Department of Meteorology

ABSTRACT

This study describes the incorporation of the Sundqvist et al. (1989) explicit non-convective cloud liquid water scheme into the Naval Research Laboratory (NRL) limited area dynamical weather prediction model. Comparisons were made between model runs with the non-convective cloud water scheme and those without the scheme to evaluate mesoscale wind pattern, longwave radiation, temperature, and cloud simulations over the U.S. West Coast for the time period 0000 UTC 02 May 1990 to 1200 UTC 03 May 1990. The most significant improvement in the updated model was the more physically realistic horizontal and vertical non-convective cloud structures produced by the cloud liquid water fields.

DTIC QUALITY INSPECTED 3

Accession For	
NTIS CRA&I	<input checked="" type="checkbox"/>
DTIC TAB	<input type="checkbox"/>
Unannounced	<input type="checkbox"/>
Justification	
By	
Distribution/	
Availability Codes	
Dist	Avail and/or Special
A-1	

TABLE OF CONTENTS

I.	INTRODUCTION	1
II.	MODEL DESCRIPTION	3
	A. GRID	3
	B. EQUATIONS.	9
	C. TIME INTEGRATION	10
	D. PARAMETERIZATIONS.	11
	E. INPUT DATA	12
III.	STRATIFORM PARAMETERIZATION.	13
	A. DESCRIPTION.	13
	B. STRATIFORM CONDENSATION.	14
IV.	WEATHER SCENARIO.	24
	A. SYNOPTIC SITUATION	24
	B. MESOSCALE FEATURES	29
V.	CONTROL MODEL SIMULATIONS.	41
	A. CATALINA EDDY.	41
	B. SOUTHERLY SURGE.	43
VI.	TEST MODEL RUN EVALUATIONS.	47
	A. MESOSCALE WIND FEATURES.	47
	B. CLOUD FRACTION	48
	C. LONGWAVE RADIATION	56
	D. TEMPERATURE.	60
	E. CLOUD LIQUID WATER	64
VII.	CONCLUSIONS AND RECOMMENDATIONS.	70
	A. CONCLUSIONS.	70
	B. RECOMMENDATIONS.	72
	REFERENCES	74
	INITIAL DISTRIBUTION LIST.	76

ACKNOWLEDGMENTS

I would like to thank Russ Schwanz for all his help with my IDEA lab files and to Steve Drake for answering all of my endless questions on the VISUAL display program. Thanks also to Mark Boothe for always getting the last-minute computer equipment I needed. My thanks to Professor Phil Durkee for his welcome suggestions and review of this thesis. Finally, my sincerest gratitude to Professor Teddy Holt for his continued patience, support, and guidance during this study and throughout my time at NPS.

This research was funded by the NPS Direct Merit Funding.

I. INTRODUCTION

The Naval Research Laboratory (NRL) Limited Area Dynamical Weather Prediction Model is an evolving research model for testing new methods of modeling various mesoscale phenomena. The model has shown success in resolving topographic and coastal features. Also, high vertical resolution in the lower levels of the model has allowed close examination of processes occurring within the boundary layer. Previous studies (Grandau 1992 and Stewart 1992) have demonstrated the NRL model's effectiveness in resolving mesoscale and boundary layer features in this region.

The United States West Coast poses a big modeling challenge due to its topographic features and coastal mesoscale phenomena such as the Catalina eddy and the southerly surge. In addition, much of the California coast experiences frequent stratus clouds which can significantly affect the weather in the region.

The stratiform condensation (or non-convective) process is important in modeling coastal mesoscale phenomena. A very simplistic approach is to represent cloud cover as being either total or zero for each grid box depending on whether gridpoint relative humidity has reached 100% or not. A more advanced technique would be to parameterize the process on the subgrid scale. Cloud cover (or cloud

fraction) could be determined more realistically as a function of gridpoint relative humidity and a relative humidity threshold or critical value.

This study examines the incorporation of the stratiform condensation process of Sundqvist et al. (1989) into the NRL limited area mesoscale model. Previous NRL model simulations by Stewart (1992) included cloud fractions as determined by the method of Slingo and Ritter (1985). These simulations, hereafter referred to as the "control" case, will be compared to the NRL model incorporating the Sundqvist et al. explicit non-convective cloud liquid water scheme, hereafter referred to as the "test" case. The inclusion of cloud water as a variable in predicting stratiform clouds is a major feature of Sundqvist's scheme.

Section II describes the NRL mesoscale model and the extent of the geographic region involved. Section III outlines the Sundqvist et al. stratiform parameterization technique. Section IV is the regional weather scenario for the time period including specific mesoscale phenomena. Section V describes the mesoscale structure of the control model simulations. Section VI evaluates the test model runs in comparison to the control model, and Section VII includes conclusions and recommendations.

II. MODEL DESCRIPTION

The Naval Research Laboratory (NRL) regional weather prediction model is a quasi-hydrostatic, baroclinic, mesoscale model which incorporates cumulus, boundary layer, and radiation parameterizations. This limited area model is most appropriate where near-gradient balance of large scale motions in the lower troposphere exists.

Since the isobaric coordinate system does not easily handle varying topography, the vertical coordinate sigma (σ) is used. This is defined as the ratio of pressure to the surface pressure.

$$\sigma = \left(\frac{P}{P_s} \right) \quad (2.1)$$

Specifics of the NRL model are detailed by Madala et al. (1987). The basics are outlined in the following pages.

A. GRID-

The horizontal grid is a staggered Arakawa C-grid. This type of network is best for the simulation of wind field geostrophic adjustment and conservation of integral properties. General curvilinear horizontal coordinates with user specified horizontal grid spacing is used. For an M X N field ($i=1,2,\dots,M$; $j=1,2,\dots,N$), temperature (T),

geopotential height (Φ), specific humidity (q), and sigma (σ) are computed at mass points (i,j), with u -velocity (east-west) and v -velocity (north-south) computed at the midpoints along the x - and y -axis respectively (See Figure 1).

The horizontal domain is a 103 X 91 grid with 1/6 degree resolution in latitude and longitude from 28° N to 43° N and 113° W to 130° W. Figure 2A shows the extent of this region along with points of interest referred to for profile and cross-sectional plots in this study and Figure 2B displays main geographic points of reference. Model simulations employ 23 vertical sigma levels as shown in Table 1. Thirteen of these layers are below 850 mb ensuring a high vertical resolution within the boundary layer.

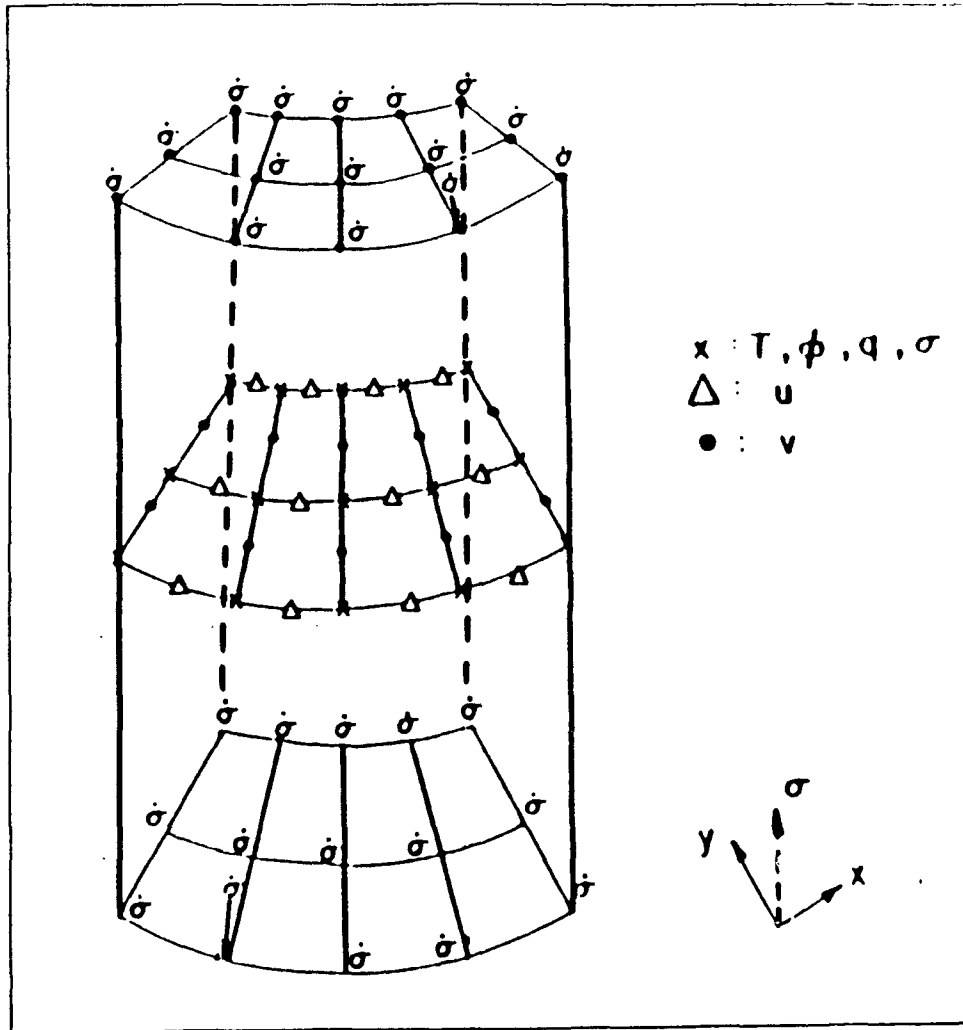
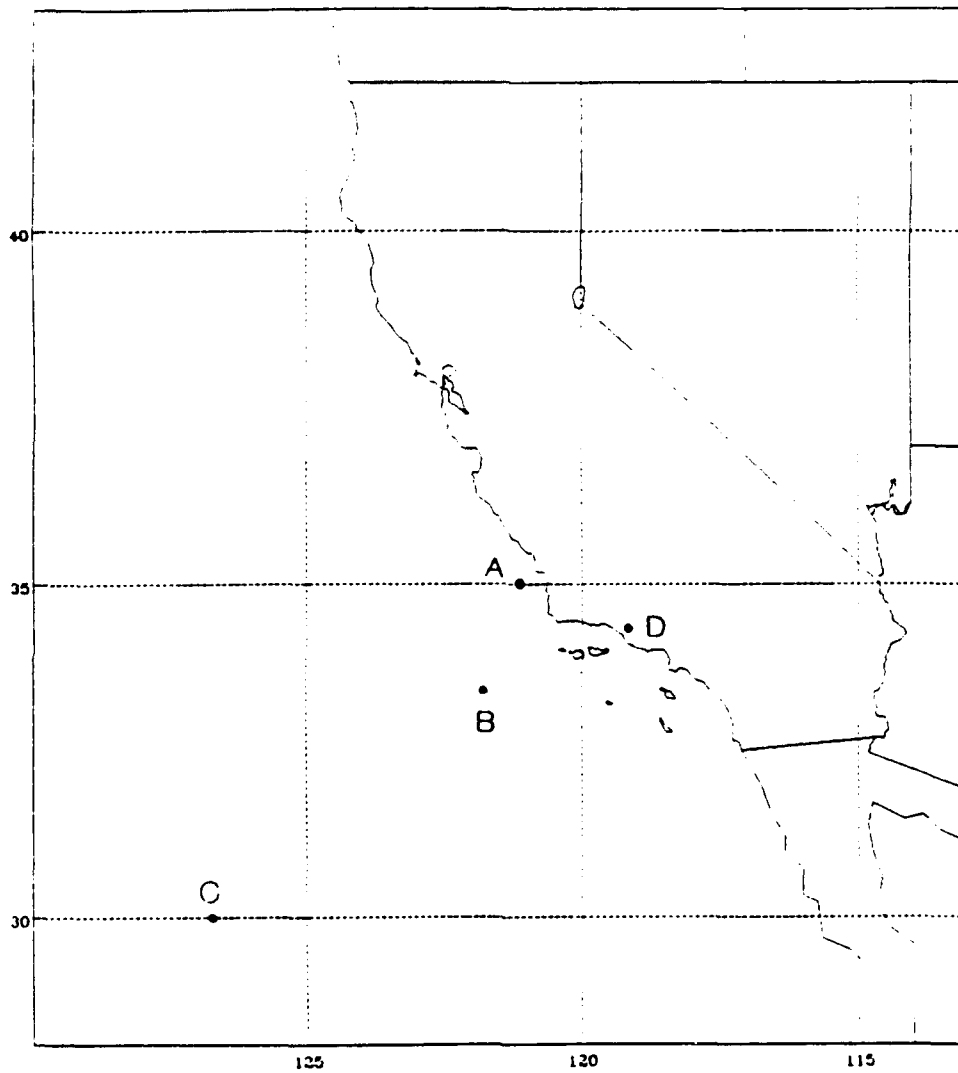


Figure 1
 Horizontal and vertical grid network
 utilized in the NRL mesoscale model

(Madala et al. 1987)



Point 'A' (35N,121W)
Point 'B' (33N,122W)
Point 'C' (30N,127W)
Point 'D' (34N,119W)

Figure 2A
NRL model horizontal domain.

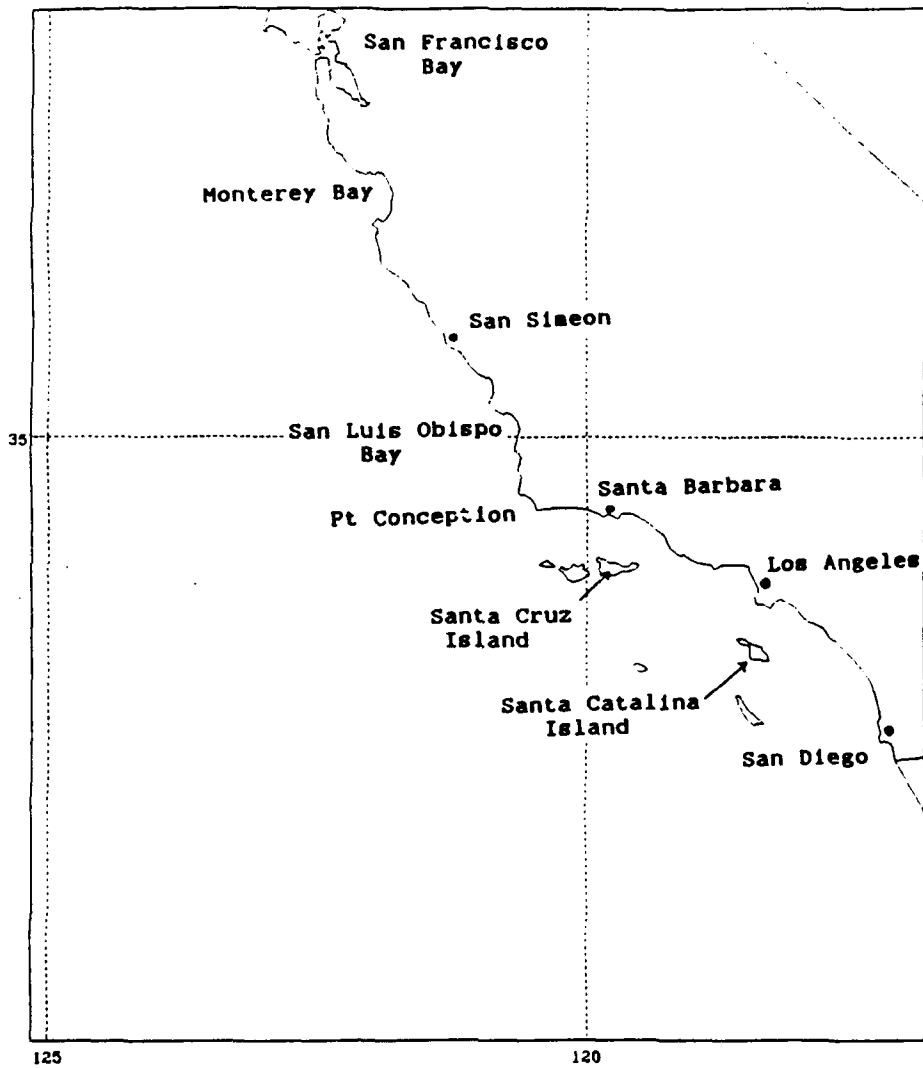


Figure 2B
Significant geographic points.

TABLE 1
MODEL SIGMA LEVELS

Model Level	Sigma (σ)
1	0.05
2	0.15
3	0.25
4	0.35
5	0.45
6	0.55
7	0.64
8	0.715
9	0.78
10	0.835
11	0.88
12	0.915
13	0.94
14	0.957
15	0.969
16	0.978
17	0.985
18	0.99
19	0.9935
20	0.996
21	0.99775
22	0.998
23	0.99975

B. EQUATIONS-

The governing primitive equations are formulated in surface pressure flux forms (i.e. $p_s u$, $p_s v$, etc.). The dynamic system consists of seven equations, five of which are prognostic, and two which are diagnostic. (See Madala, 1987 for the complete form of the equations).

u- & v-momentum equations:

$$\frac{\partial}{\partial t} (p_s u) \quad (2.2)$$

$$\frac{\partial}{\partial t} (p_s v) \quad (2.3)$$

thermodynamic equation:

$$\frac{\partial}{\partial t} (p_s T) \quad (2.4)$$

moisture continuity equation:

$$\frac{\partial}{\partial t} (p_s q) \quad (2.5)$$

surface pressure tendency equation:

$$\frac{\partial}{\partial t} (p_s) \quad (2.6)$$

hydrostatic equation:

$$\frac{\partial \phi}{\partial \sigma} \quad (2.7)$$

continuity equations:

$$\frac{\partial}{\partial \sigma} (p_s \sigma) \quad (2.8)$$

A closed system is formed for the dependent variables u , v , T , q , p_s , ϕ , and σ (vertical velocity).

C. TIME INTEGRATION-

The split-explicit method is utilized which effectively splits terms in the prognostic equations into two parts: those governing the Rossby modes and those governing the faster gravity modes. For quasi-linear gravity modes, the pressure gradient and divergence terms vary faster than the remaining terms. This allows that part of the equation with these remaining terms to use a larger time step. The split equations are integrated with time steps for their respective CFL criteria.

D. PARAMETERIZATIONS-

The model parameterizes a number of physical processes including cumulus precipitation, planetary boundary layer (PBL) processes, and radiation.

Cumulus parameterization is from the modified Kuo scheme (Kuo 1974). Surface layer parameterization is based on Monin-Obukhov similarity theory. PBL parameterization is with turbulent kinetic energy (TKE) closure described in Holt and Raman (1988).

The radiation parameterization incorporated in the model is the Harshvardhan et al. (1987) scheme. Stewart's (1992) study parameterizing longwave and shortwave effects showed the improvements in the model's ability to simulate diurnal and cloud-related radiative processes.

The cloud parameterization scheme incorporated in the control model by Stewart (1992) is based on cloud fractions using a modified Slingo and Ritter (1985) method where average layer relative humidities are compared to critical relative humidity values. This method produces stable and convective cloud fractions for a horizontal grid at each sigma layer. The clouds are diagnosed as either stratiform or cumulus.

Due to the frequent presence of stratiform clouds along the west coast, the need for a more sophisticated non-convective parameterization scheme is clear. This

stratiform parameterization is discussed in detail in Section III.

E. INPUT DATA-

Data for the period 0000 UTC 02 May - 1200 UTC 03 May 1990 was taken from the Navy Operational Global Atmospheric Prediction System (NOGAPS). Model initialization data was retrieved from archived Fleet Numerical Oceanography Center's 2.5 degree global analyses and horizontally and vertically interpolated to the NRL model resolution (Grandau 1992). Fields include u- and v- components of velocity, temperature (T), vapor pressure, sea level pressure, and sea surface temperature (SST).

III. STRATIFORM PARAMETERIZATION

A. DESCRIPTION-

Increased development of mesoscale atmospheric modeling has resulted in a more involved look at the proper treatment of the stratiform condensation process. The high occurrence of stratus clouds along the U.S. West Coast and its effect on regional weather patterns makes this region ideal for this type of study.

One assumption typically made in representing stratiform condensation is that the gridpoint relative humidity must reach 100% in order for condensation to occur. This results in a simplistic approach of cloud cover either being represented as zero or 100% at individual grid points. A more realistic treatment of this case would be a subgrid scale method requiring a parameterization of the process.

Sundqvist et al. (1989) devised a treatment of condensation cloud processes for convective and non-convective precipitation. This study will only incorporate Sundqvist's non-convective scheme. The convective case utilizes the scheme by Kuo (1974) adopted to account for the inclusion of cloud water as a prognostic variable. The

first step in the parameterization of convective and non-convective precipitation is a stability check of the grid column. The criterion here is that an air parcel at the surface should be positively buoyant after reaching the lifting condensation level (LCL). If the column is conditionally unstable, the Kuo scheme (without Sundqvist's modifications) is used. If not, the possibility of stratiform condensation is investigated. The Sundqvist et al. stratiform condensation treatment is described in the following pages.

B. STRATIFORM CONDENSATION-

For stratiform condensation to take place, a relative humidity threshold value (of less than unity) within a grid box must be exceeded. Parameterization of the stratiform condensation process is a function of quantities such as stability, cloudiness, altitude, and type of surface. The prognostic equations used are those for cloud water mixing ratio (m), temperature (T), and specific humidity (q).

Changes in cloud water are due to local changes in m from advection and diffusion (A_{\cdot}), latent heat release (Q), local rate of release of precipitation (P), and evaporation

of cloud water to vapor advected to a grid box where no condensation is occurring (E_c). In equation form,

$$\frac{\partial m}{\partial t} = A_n + Q - P - E_c \quad (3.1)$$

where $\partial m / \partial t$ is total cloud water mixing ratio tendency. The local rate of release of precipitation (P) is dependent upon a cloud liquid water threshold value (m_c). Efficient release of precipitation occurs when m exceeds the cloud fraction multiplied by this threshold value.

$$P = c_o m \left[1 - e^{-\left(\frac{m}{m_c}\right)^2} \right] \quad (3.2)$$

c_o is characteristic conversion rate of cloud particles to precipitation size, and b is the cloud fraction.

The cloud fraction is determined from the relative humidity (RH), a relative humidity threshold value for condensation (RH_c), and the weighted average of the humidity of the cloudy part (RH_s). (RH_s is defined to equal the value of 1).

$$b = 1 - \sqrt{\frac{(RH_s - RH)}{(RH_s - RH_c)}} \quad (3.3)$$

Typically, RH_c values are empirically derived. Sundqvist et al. (1989) used RH threshold values above the boundary layer of:

- 0.75 -- over land, and
- 0.85 -- over the ocean.

In the boundary layer, RH_c is assumed to linearly approach unity at the surface. Subgrid-scale topography effects are taken into account by assuming the value of RH_c to be 0.1 lower over the land than over the ocean. Also, to prevent the unrealistically early formation of cirrus clouds, RH_c is increased asymptotically toward unity for temperatures less than 238° K. Figure 3 depicts the Sundqvist et al. relative humidity threshold profile.

This is contrasted with the approach by Slingo and Ritter (1985) and used by Stewart (1992) in the control model simulations. Here, different critical relative humidity values are computed as a function of sigma. For each model sigma level, a critical relative humidity is determined from the equation:

$$RH_c = 1 + 2(\sigma^2 - \sigma) + \sqrt{3}\sigma(1 - 3\sigma + 2\sigma^2) \quad (3.4)$$

In order to account for the lack of model-simulated clouds near the coastal regions, Stewart used satellite imagery to propose a modification of critical relative humidity values for this particular 2-3 May 1990 case study.

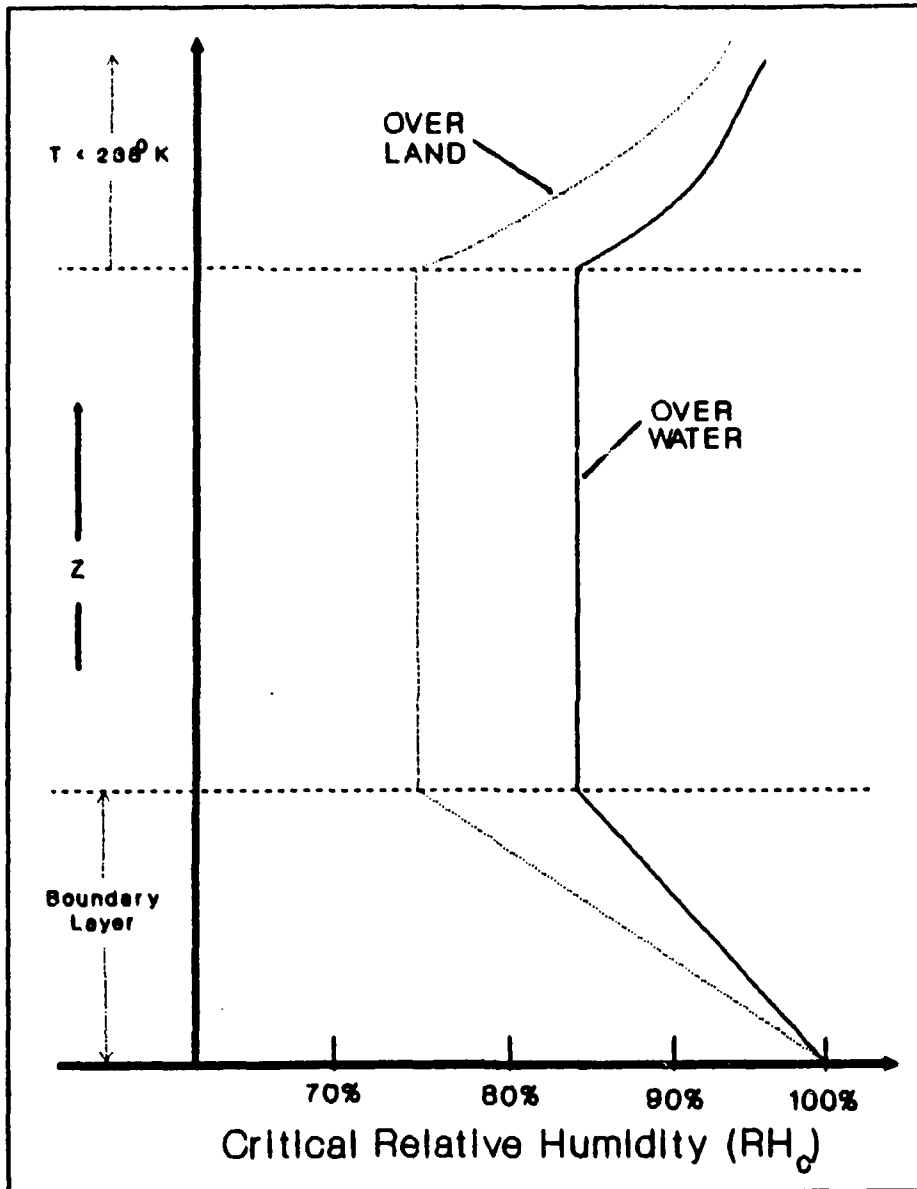


Figure 3
 Critical Relative Humidity Profiles
 (Sundqvist et al. 1989)

Figure 4 shows the representations of critical relative humidity values by both Slingo et al. and Stewart.

For stratiform clouds, the evaporation of precipitating water to vapor as it falls through subsaturated air (E_r) depends on cloud fraction (b), relative humidity (RH), and a layer-averaged precipitation rate (\bar{P}).

$$E_r = k_E (RH_s - RH) (1-b) \sqrt{\bar{P}} \quad (3.5)$$

k_E is a coefficient expressing the instantaneous evaporation of advected m.

Temperature changes are due to the temperature tendency from advection, diffusion, and radiation (A_T), latent heat release (Q), evaporation of precipitating water to vapor (E_r), and evaporation of advected cloud liquid water (E_c).

$$\frac{\partial T}{\partial t} = A_T + \left(\frac{L}{c_p}\right) Q - \frac{L}{c_p} (E_c + E_r) \quad (3.6)$$

c_p in this equation is the specific heat of dry air at constant pressure, and L is latent heat of vaporization.

The change in specific humidity ($\partial q / \partial t$) comes from the effects of advection and diffusion (A_q), latent heat release (Q), and evaporation ($E_c + E_r$).

$$\frac{\partial q}{\partial t} = A_q - Q + E_c + E_r \quad (3.7)$$

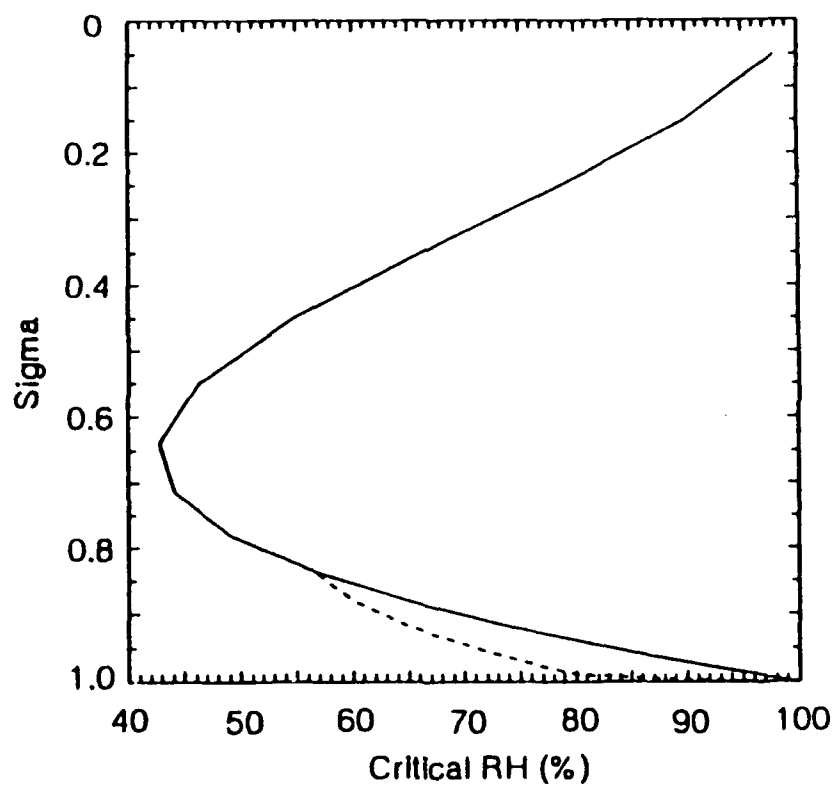


Figure 4
Critical relative humidity profiles.

(Slingo & Ritter -- solid)

(Stewart -- dashed)

(Stewart 1992)

Combining the prognostic equations for temperature and specific humidity with the Clausius-Clapeyron equation (Sundqvist 1988) gives an expression for Q .

$$Q = \frac{M - q_s \left[\frac{\partial(RH)}{\partial t} \right]}{1 + \frac{(RH) e L^2 q_s}{R C_p T^2}} \quad (3.8)$$

where M is the convergence of available latent heat given as:

$$M = A_q - \frac{(RH) e L q_s}{R T^2} (A_r) + \frac{(RH) q_s}{p} \left(\frac{\partial p}{\partial t} \right) \quad (3.9)$$

q_s is saturation specific humidity,

ϵ is the ratio of molecular weight of vapor to molecular weight of dry air ($=0.622$), and

R is the gas constant for dry air.

Hence, positive advection of A_q and pressure tendency ($\partial p / \partial t$) would tend to increase available latent heat convergence, while warm advection ($A_r > 0$) would tend to decrease convergence.

To close the system, the tendency of RH can be expressed by:

$$\frac{\partial(RH)}{\partial t} = \frac{2(1-b)(RH_s - RH_c) [(1-b)M + E_r]}{2q_s(1-b)(RH_s - RH_c) + \left(\frac{m}{b}\right)} \quad (3.10)$$

At this point, temperature and specific humidity tendencies ($\partial T / \partial t$ and $\partial q / \partial t$) can be computed. The mixing

ratio tendency ($\partial m / \partial t$) is obtained by semi-implicit time integration of equation (3.1), which may be rewritten as:

$$\frac{\partial m}{\partial t} = RHS - P \quad (3.11)$$

$$\frac{\partial m}{\partial t} = RHS - c_o m \left[1 - e^{-\left(\frac{m}{bm_r}\right)^2} \right] \quad (3.12)$$

(RHS = right hand side)

And in finite difference form:

$$m^{n+1} = m^{n-1} + 2\Delta t (RHS) - 2\Delta t c_o \bar{m} \left[1 - e^{-\left(\frac{\bar{m}}{bm_r}\right)^2} \right] \quad (3.13)$$

$$\bar{m} = \frac{1}{2} (m^{n+1} + m^{n-1}) \quad (3.14)$$

Resulting in a non-linear equation,

$$x[1 + \Delta t c_o (1 - e^{-x^2})] = \frac{m^{n-1} + (RHS) \Delta t}{bm_r} \quad (3.14)$$

$$\left(x = \frac{\bar{m}}{bm_r} \right) \quad (3.15)$$

which may be solved using the Newton-Raphson iteration method.

Table 2 provides a summary of various stratiform condensation processes described by the tendency equations and their influences. Water vapor condensing into cloud

TABLE 2
SUMMARY OF STRATIFORM CONDENSATION PROCESSES

SPECIFIC HUMIDITY TENDENCY:

$$\frac{\partial q}{\partial t} = A_q - Q + E_o + E_r$$

TEMPERATURE TENDENCY:

$$\frac{\partial T}{\partial t} = A_T + \frac{L}{\sigma_p} Q - \frac{L}{\sigma_p} E_o + \frac{L}{\sigma_p} E_r$$

CLOUD WATER MIXING RATIO TENDENCY:

$$\frac{\partial m}{\partial t} = A_m + Q - P - E_o$$

PROCESS	SIGNIFICANT TERM	q, T, m TENDENCY
q condenses to m	Q	q T m
m advected & evaporates to q	E _o	q T m
precipitation evaporates to q	E _r	q T m —
m precipitates out	P	q — T — m

liquid water results in a decrease in specific humidity (q), and an increase in temperature (T) and cloud liquid water (m). When cloud water is advected and evaporated into water vapor, specific humidity is increased, while temperature and cloud liquid water are decreased. For the case where precipitation evaporates to vapor, specific humidity is increased and temperature is decreased. Finally, for cloud water precipitating out, cloud liquid water decreases, with specific humidity and temperature remaining constant.

IV. WEATHER SCENARIO

A. SYNOPTIC SITUATION:

1. Upper Air-

The period of interest for this study is 0000 UTC 02 May 1990 to 1200 UTC 03 May 1990. A high pressure ridge dominated the eastern Pacific region and slowly intensified during the period. A closed upper level low that was situated over southern Arizona initially deepened and subsequently filled and moved eastward over the latter part of the period.

There was also evidence of a weak shortwave moving over the Pacific Northwest at the start of the period. Figures 5A to 5D show the 500 mb pattern for the period.

2. Surface-

During this period, a weak low pressure area originating in the north central Pacific deepened and moved to the northeast. This low pressure cell eventually reached the British Columbia coast at the end of the period.

A closed high pressure cell was located in the eastern Pacific off the northern California coast ridging

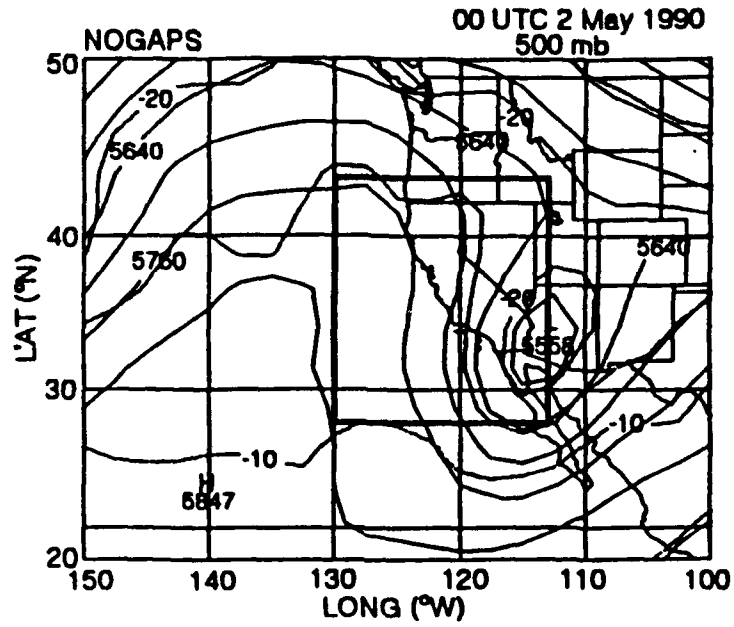


Figure 5A
0000 UTC 02 May 1990
NOGAPS 500 mb Analysis
heights (solid, m)
temperature (dashed, °C)

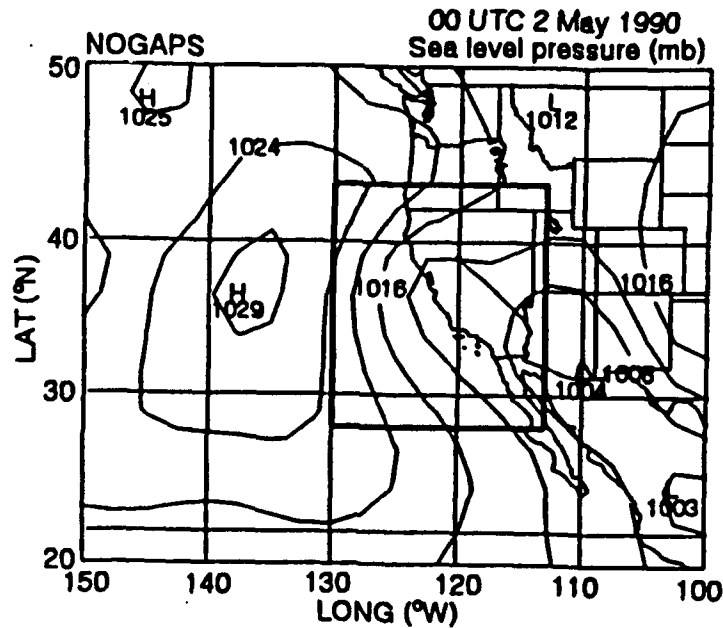


Figure 6A
0000 UTC 02 May 1990
NOGAPS Sea Level Pressure Analysis

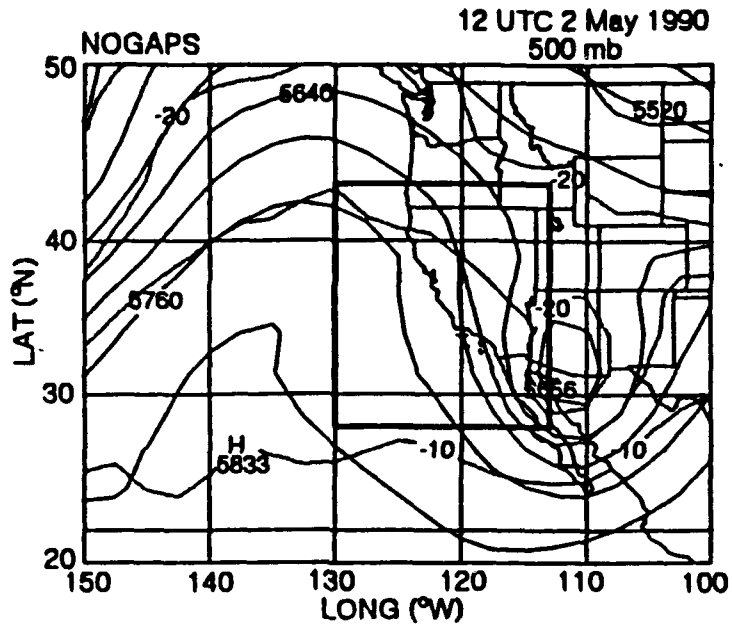


Figure 5B
1200 UTC 02 May 1990
NOGAPS 500 mb Analysis
heights (solid, m)
temperature (dashed, °C)

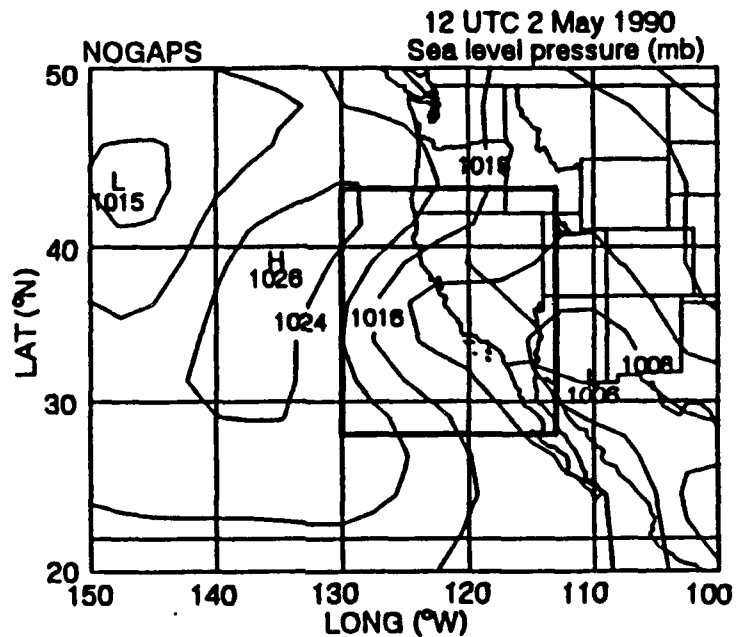


Figure 6B
1200 UTC 02 May 1990
NOGAPS Sea Level Pressure Analysis

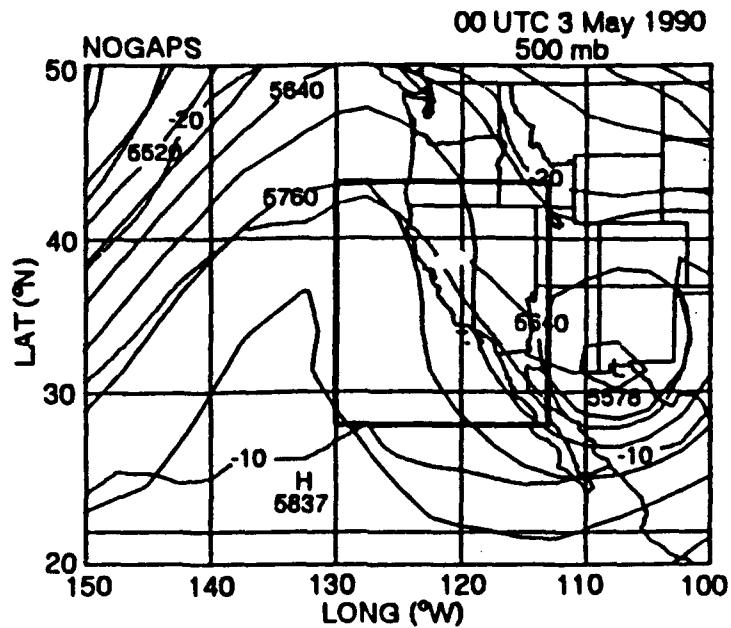


Figure 5C
0000 UTC 03 May 1990
NOGAPS 500 mb Analysis
heights (solid, m)
temperature (dashed, °C)

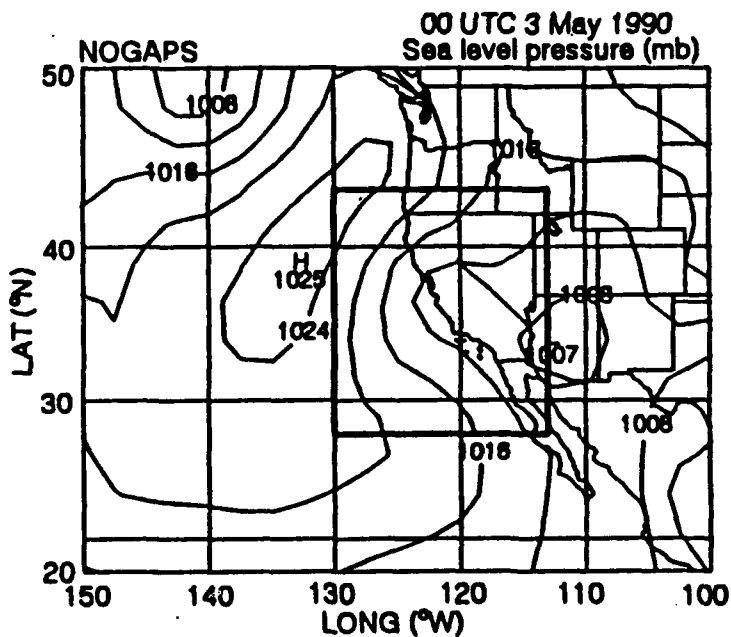


Figure 6C
0000 UTC 03 May 1990
NOGAPS Sea Level Pressure Analysis

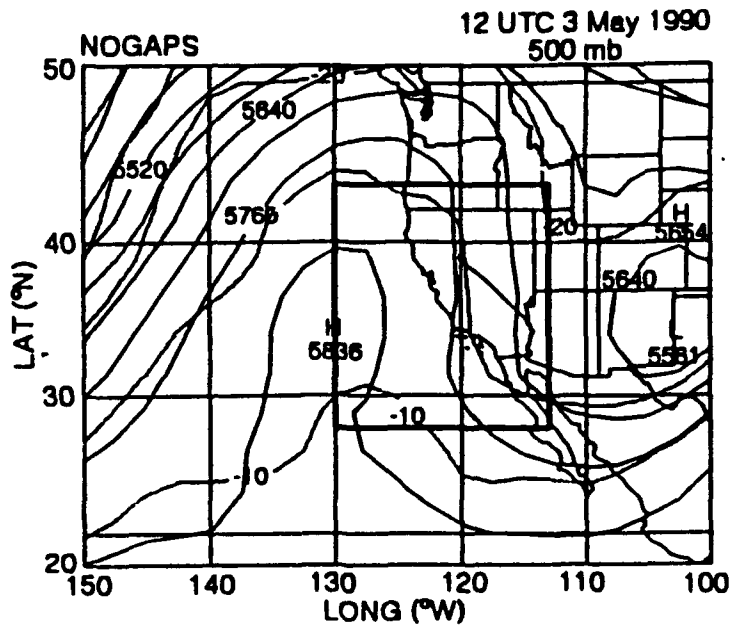


Figure 5D
1200 UTC 03 May 1990
NOGAPS 500 mb Analysis
heights (solid, m)
temperature (dashed, °C)

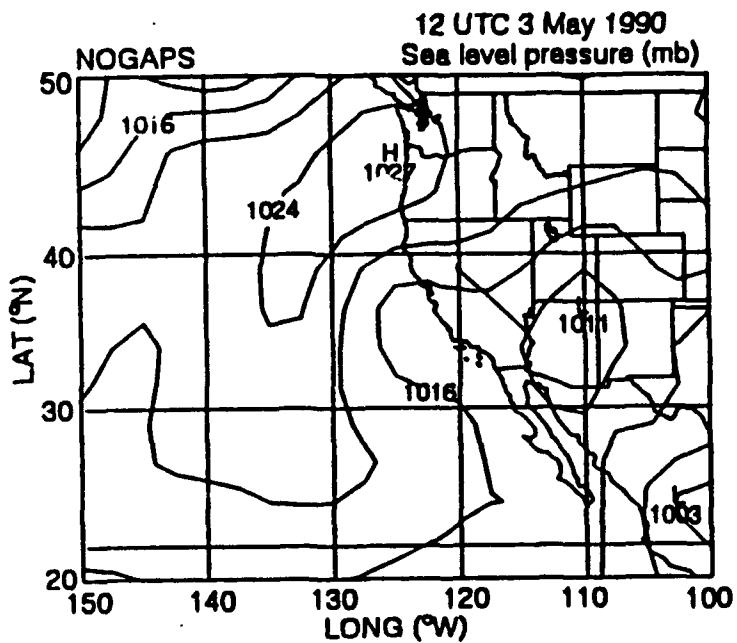


Figure 6D
1200 UTC 03 May 1990
NOGAPS Sea Level Pressure Analysis

into the Pacific Northwest. The high pressure pattern continually weakened while gradually moving northeastward toward the Washington coast.

A thermal low remained over Arizona and filled slightly during the period. This low had an associated inverted trough extending over the California coast. (See Figures 6A to 6D).

B. MESOSCALE FEATURES:

Specific mesoscale features of interest for the region during the period include the land and sea breeze, the Catalina eddy, and the southerly stratus surge. Satellite images show a dominant presence of stratus along the coastlines during this time period. Because of the close association of stratus clouds with the latter two features, this study concentrates on the Catalina eddy and the southerly surge.

1. Catalina Eddy-

The Catalina eddy is a feature typically occurring from late spring to early fall characterized by surface wind cyclonic circulation in the vicinity of Santa Catalina Island. Figure 7, from Mass et al. (1989), is a Catalina eddy composite of 1200 UTC surface winds (knots) and sea

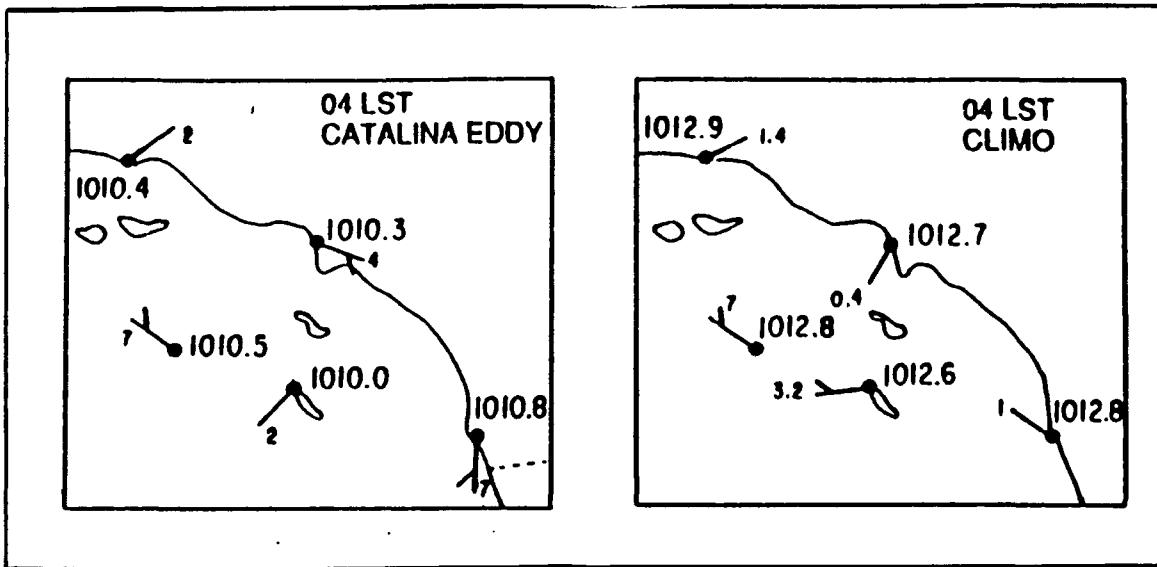


Figure 7
 1200 UTC Catalina Eddy and climatology
 composite of surface winds (knots) and
 sea level pressure (millibars).

(Catalina eddy composite based on 50 events;
 climatology composite based on data for May
 through September 1964-1982)

(Mass and Albright, 1989)

level pressure (mb) compared with climatological winds and pressure.

The usual coastal southern California pattern during this period is characterized by westerly to northwesterly surface winds accompanied by morning and late evening fog and stratus. The Catalina eddy will often form when coastal winds shift to a more southerly direction. During these eddy conditions, the usual dissipation of coastal fog and stratus in the afternoon will often not happen.

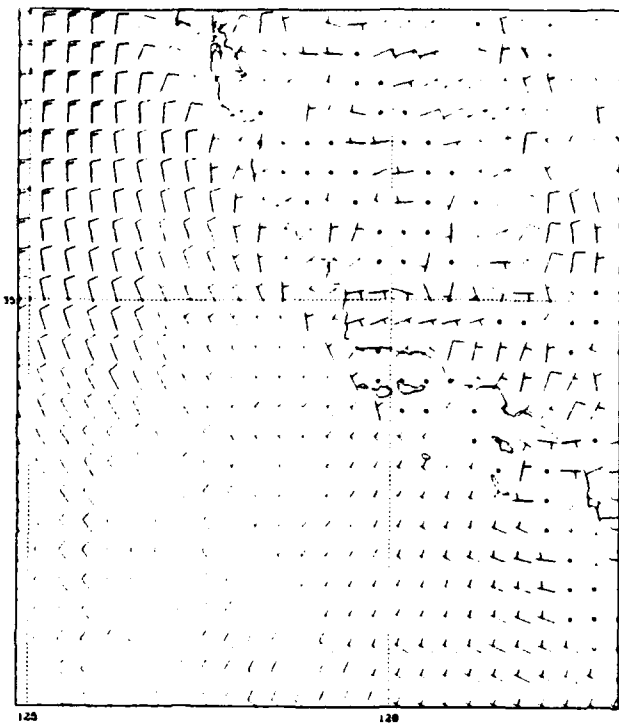
An intensified alongshore pressure gradient created by the interaction of a short wave trough with pre-existing troughs is credited by Mass et al. (1989) for this feature. Grandau (1992) found this eddy to extend upward to about 920 mb for this particular case. These eddy events can vary from a few hours to many days in duration.

2. Southerly Stratus Surge-

A phenomena along the west coast of the United States that can often be associated with the longer duration Catalina eddies is the southerly surge. A result of the alongshore pressure gradient is southerly flow developed within about 100 km (approximately one Rossby radius) of the coastal mountains. As the southerly winds maintain its flow, the cool moist marine layer is deepened, and enhanced stratus develops near the coast. The deepened marine layer

will often result in improved air quality for the Los Angeles area.

Figures 8A through 8G include surface wind observations for the period of interest. Corkill (1991) described a weak southerly surge for his study covering the same time period. Figure 8F shows southerly coastal winds from central to southern California at 2100 UTC 02 May 1990. The 2030 UTC visible satellite image (Figure 9) reveals coastal cloudiness all along the central California coast from Monterey to San Luis Obispo Bay. Dorman (1985) described the southerly surge as a result of coastally-trapped gravity currents, while Mass et al. (1989) stated that it results from a coastally trapped two-layer marine system.



Control model
1000 mb winds

(Wind speed in knots)
[short barb = 5 knots]
[long barb = 10 knots]

Surface observations

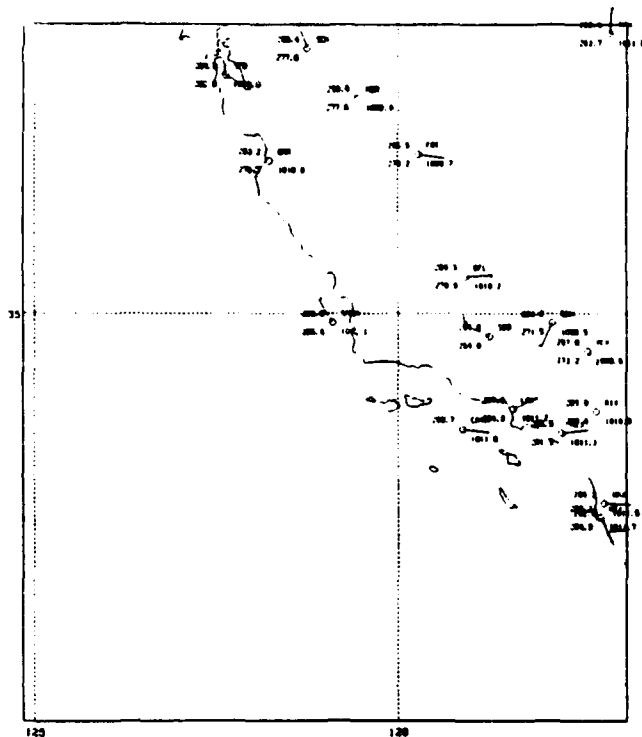
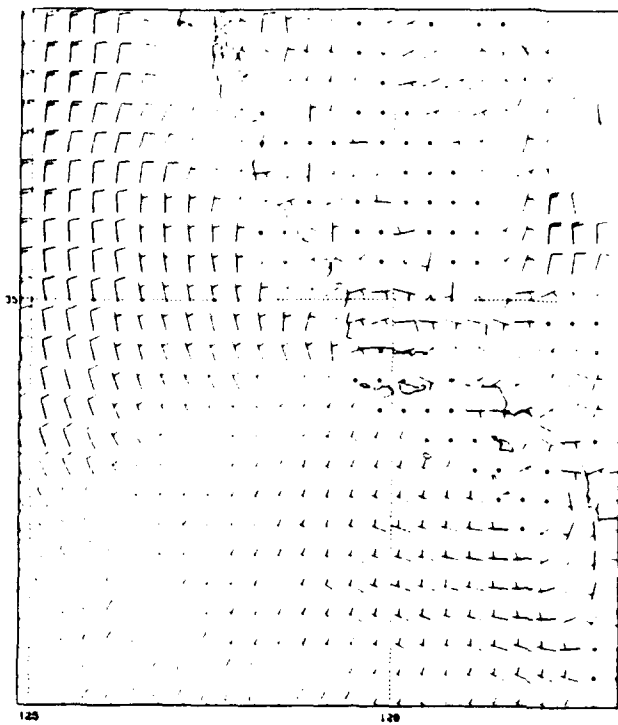
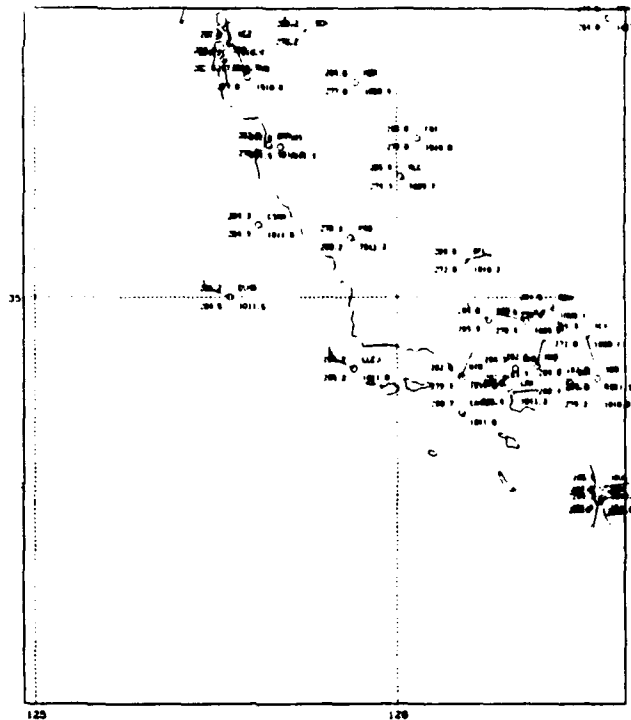


Figure 8A
0900 UTC 02 May 1990

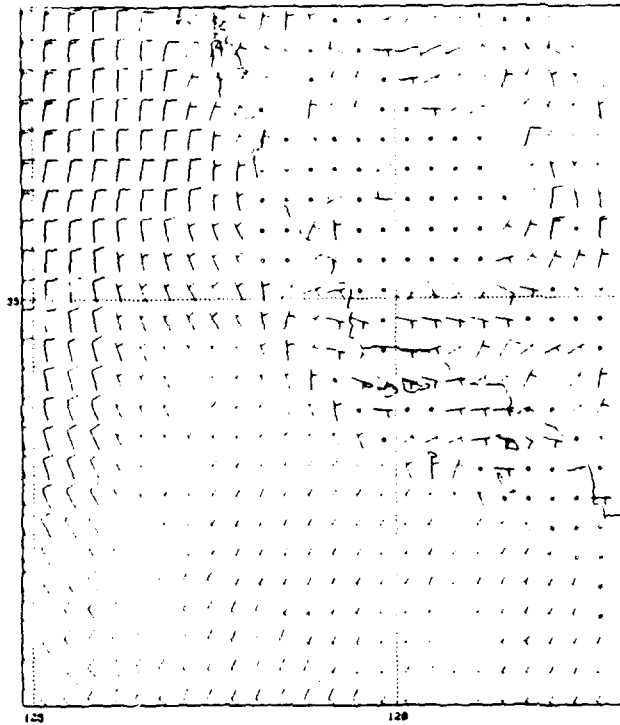


Control model
1000 mb winds

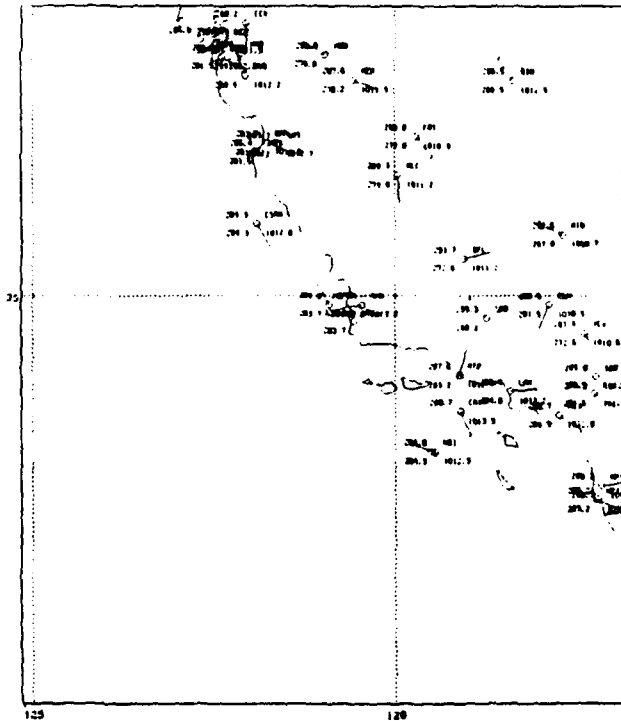


Surface observations

Figure 8B
1200 UTC 02 May 1990

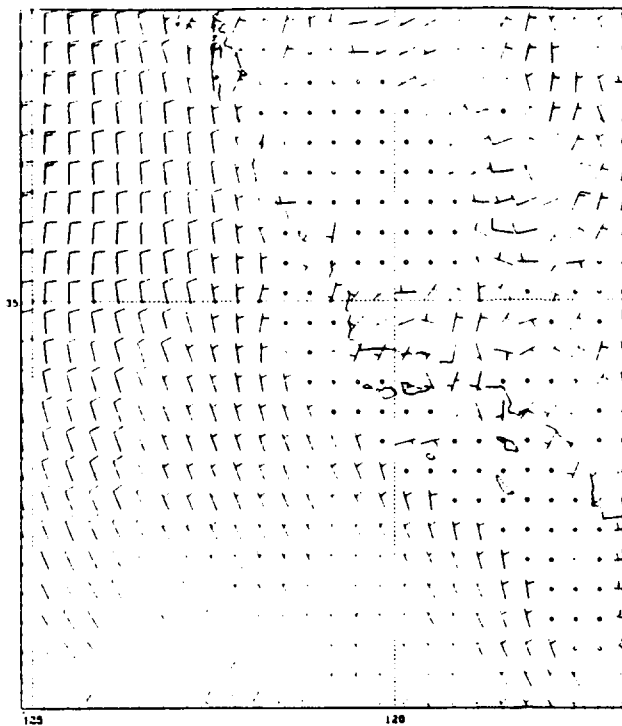


Control model
1000 mb winds

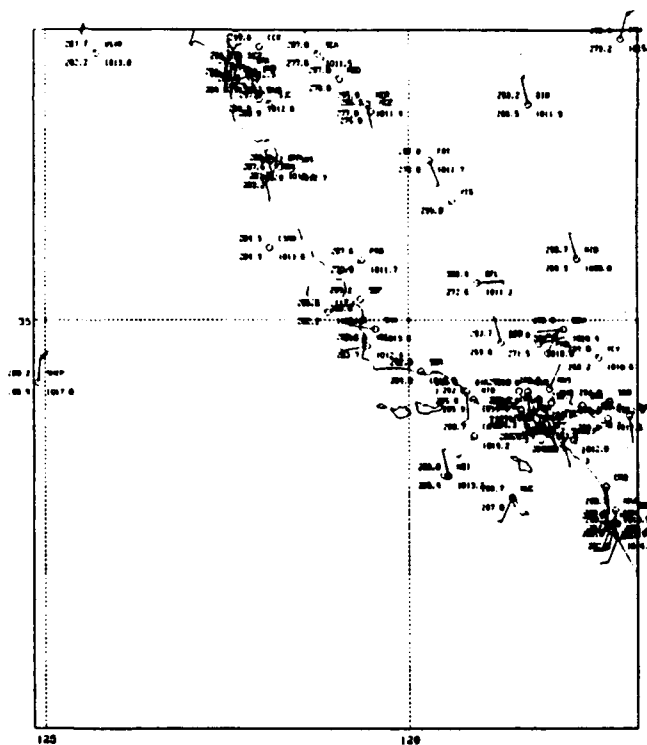


Surface observations

Figure 8C
1500 UTC 02 May 1990

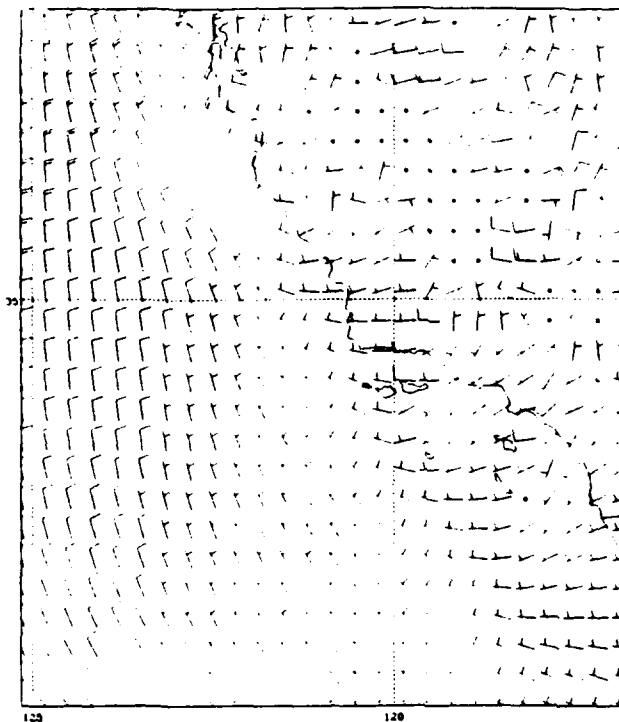


Control model
1000 mb winds

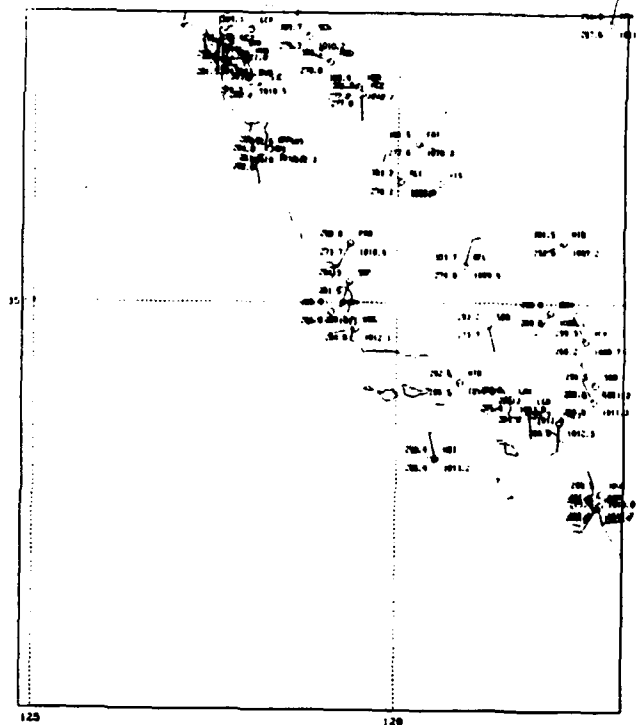


Surface observations

Figure 8D
1800 UTC 02 May 1990

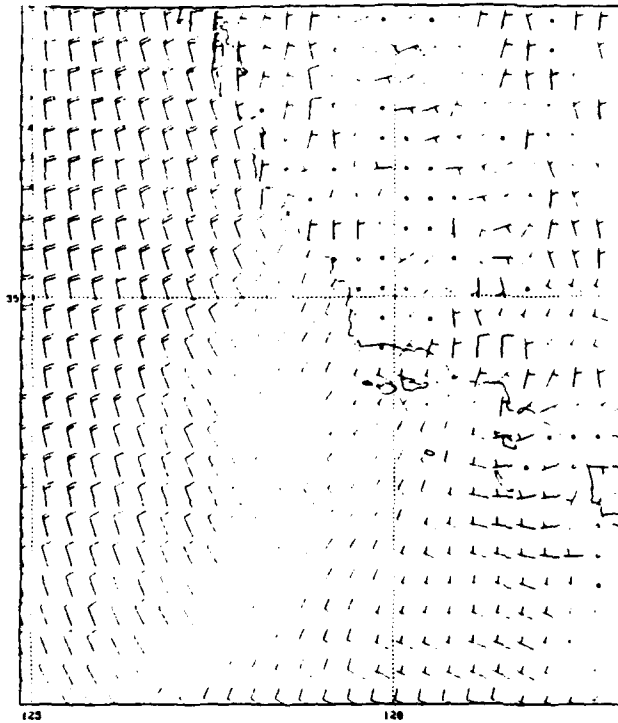


Control model
1000 mb winds

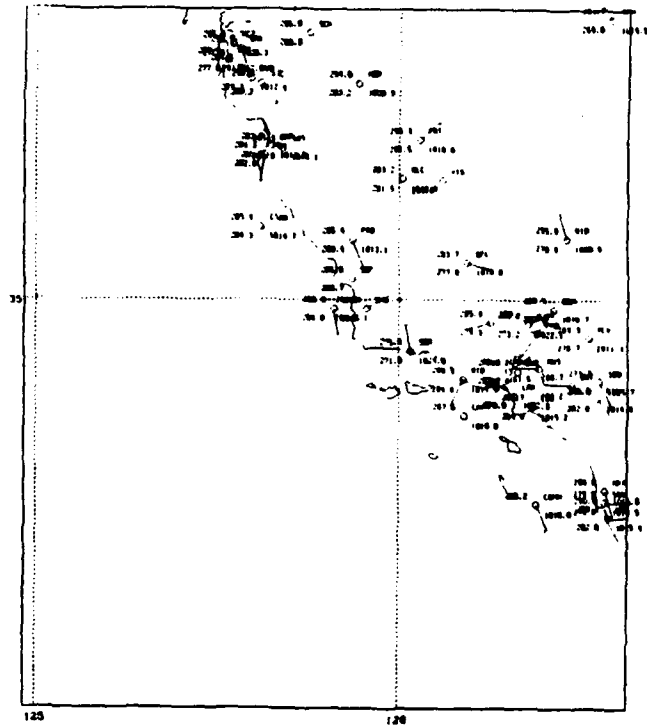


Surface observations

Figure 8B
2100 UTC 02 May 1990

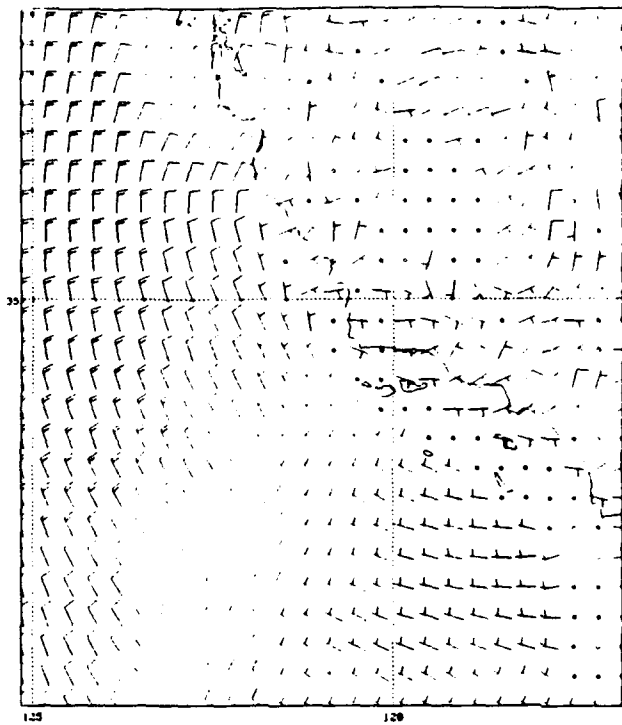


Control model
1000 mb winds

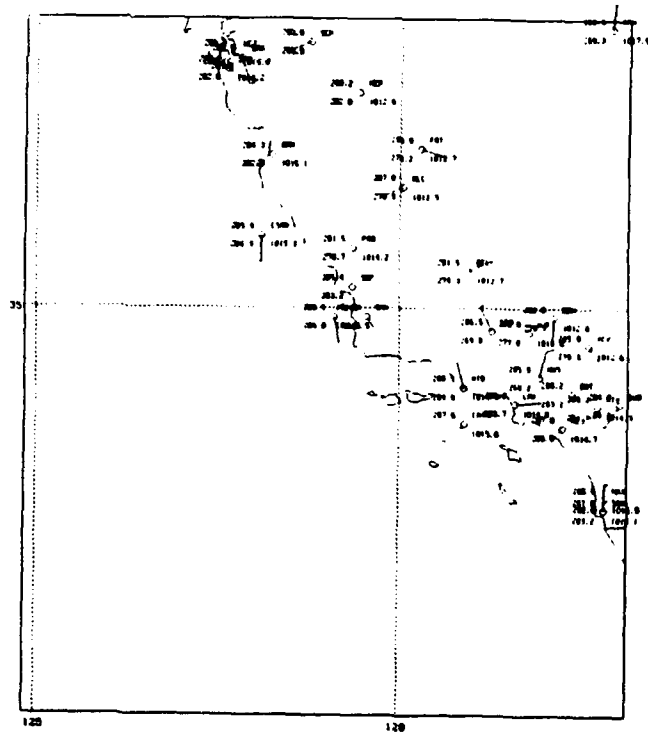


Surface observations

Figure 8F
0600 UTC 03 May 1990



Control model
1000 mb winds



Surface observations

Figure 8G
1200 UTC 03 May 1990

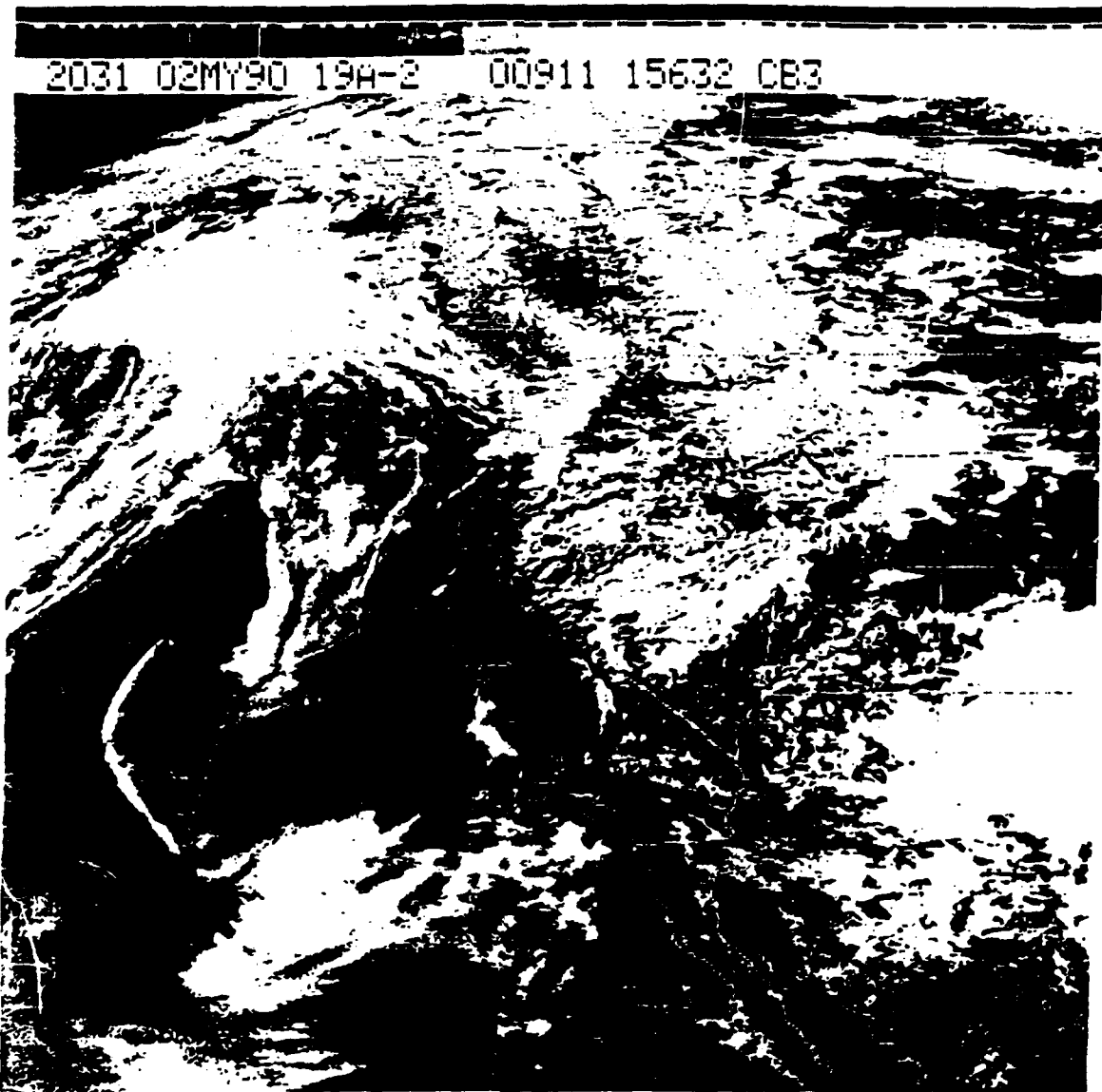


Figure 9
Visible satellite image
(2030 UTC 02 May 90)

V. CONTROL MODEL SIMULATIONS

Stewart (1992) incorporated the Harshvardhan et al. (1987) radiation parameterization into the NRL regional weather prediction model and conducted model simulations integrated for 36 hours over the time period 0000 UTC 02 May to 1200 UTC 03 May 1990. Integration over the same area and time window allows for consistent comparisons with the control model of Stewart to evaluate the impact of the new stratus parameterization.

A. CATALINA EDDY-

The control model low-level wind fields (Figures 8A to 8G) indicated clear onset of a Catalina eddy at 0900 UTC 02 May 1990 with south-southeasterly winds near San Diego and clear off-shore flow along the central to southern California coast. Further off the coast, general northerly winds were observed off Monterey Bay to west-northwesterly flow toward the Mexico border.

Three hours later, the model clearly defined the eddy pattern in the Los Angeles basin with the vortex centered between the Santa Cruz and the Santa Catalina Islands. By 1800 UTC, the pattern had become disorganized with a

transition of southerly winds extending along the coast from San Simeon to Santa Barbara.

At 2100 UTC, the winds are westerly from Pt. Conception northward, and from the southwest in the Los Angeles basin. By 0600 UTC, another eddy onset appeared to be occurring, with the 1200 UTC wind fields again giving a clear eddy pattern.

Comparison of model-predicted wind fields and a limited number of land and ship observations showed that the Catalina eddy onset appeared to be reasonably predicted. However, the model seemed to show the dissociation of the eddy sooner than the observations indicated. The 1800 UTC reports still show evidence of an eddy circulation, while the model showed mostly onshore winds along the coast. Also, observations near San Diego showed the winds maintaining more of a southerly component longer into the period (through 0600 UTC 03 May). Because of the lack of data, the reformation of another eddy later by 0600 UTC could not be readily verified.

B. SOUTHERLY SURGE-

The control model low-level wind fields (Figures 8A to 8G) showed distinct southerly coastal wind flow from San Simeon to San Diego at 1800 UTC 02 May 1990. By 2100 UTC, winds from San Simeon to Santa Barbara shifted to a predominantly western direction. From 0000 UTC 03 May 1990, winds in the area had prominent northerly components.

Observations along the coast showed southerly wind flow from Santa Barbara southward at 1800 UTC 02 May 1990. Coastal areas to the north however did not have southerly winds until 2100 UTC 02 May 1990. This coastal southerly wind flow continued up to the end of the period.

Coincident with the southerly surge time period, satellite imagery showed persistent cloudiness along the coastline from Monterey Bay to San Luis Obispo Bay. The normal late day coastal fog and stratus dissipation occurred only to the south. Persistent coastal fog and stratus with little dissipation is expected during a southerly surge stage. Figure 9 is a visible satellite image highlighting the coastal cloudiness for the region.

Time-height cross-sections for point 'A' near San Luis Obispo Bay (35° N, 121° W) showed model southerly winds near the surface at around 1800 UTC 02 May time period. Figure 10 shows the southerly surface flow isolated during that time window (dashed lines indicate northerly winds while

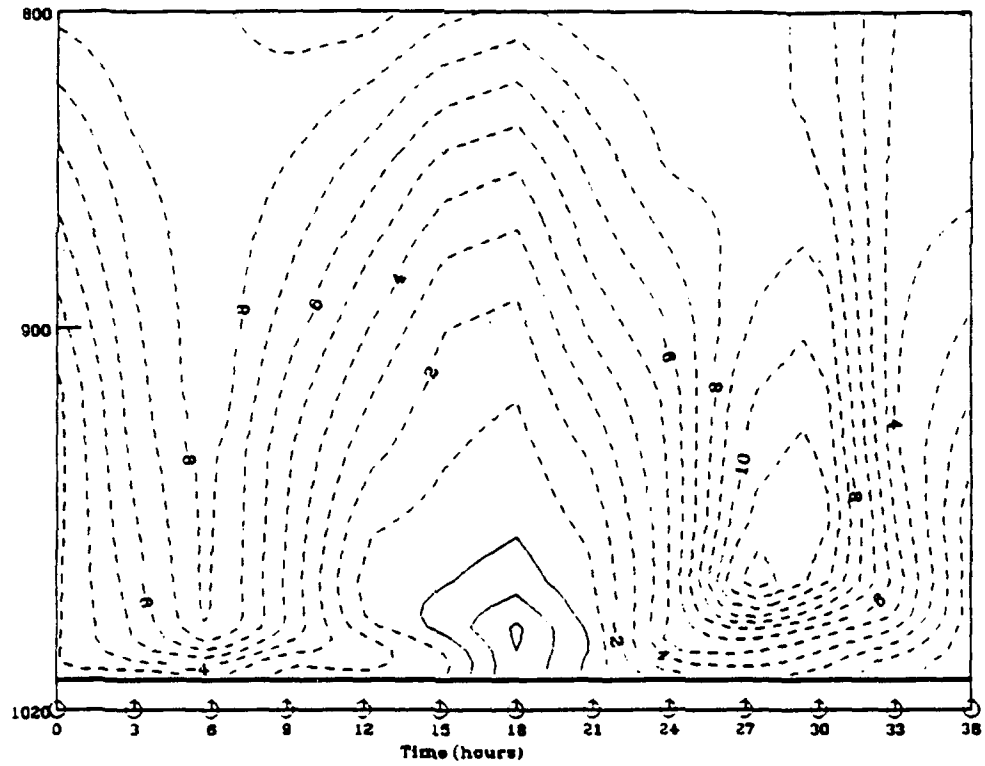
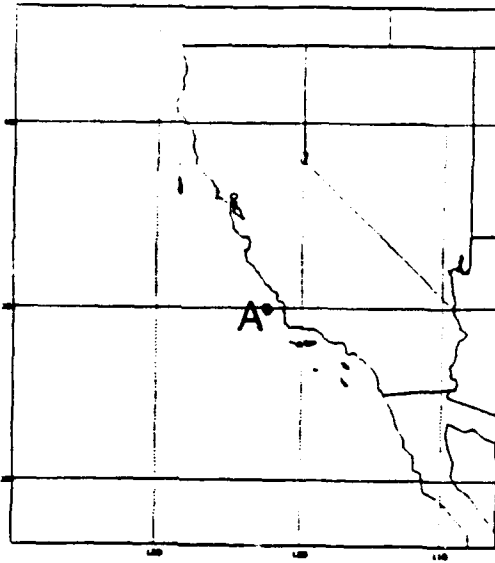


Figure 10
Control model time-height cross-section of southerly (v-component) winds (m/s) at Point 'A'.

solid lines are southerly). Also, the model revealed a local maxima in humidity in the lowest 200 meters at around 1800 UTC agreeing with the expected moist marine layer that develops from the southerly surge. Figure 11 highlights the high moisture near the surface for that particular time period.

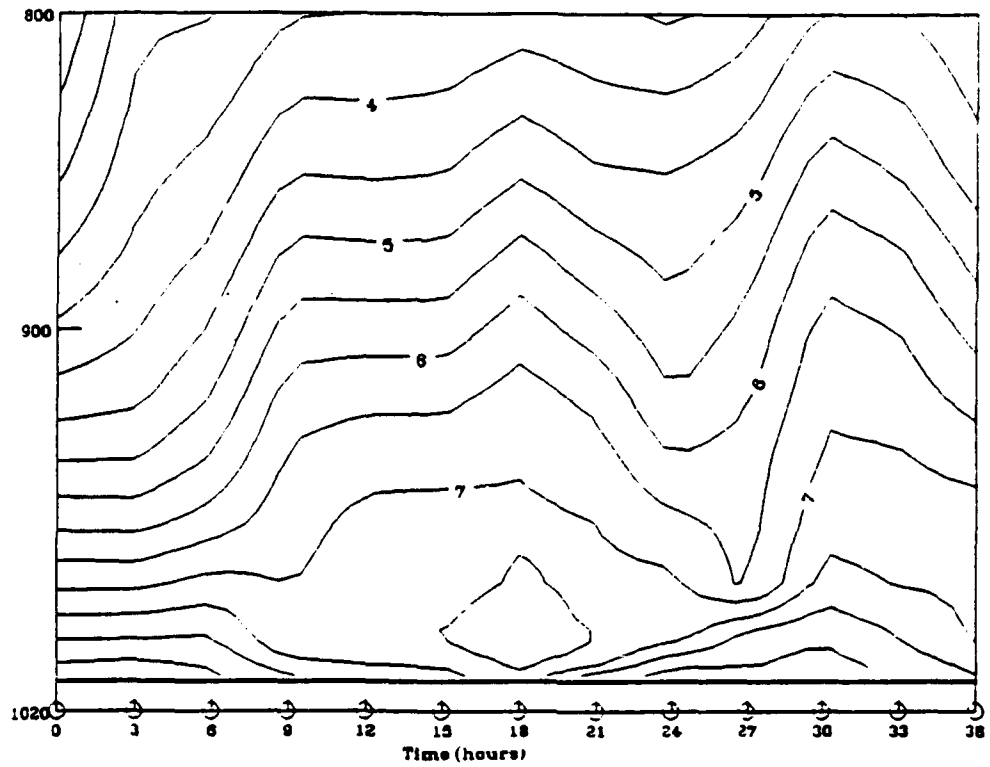
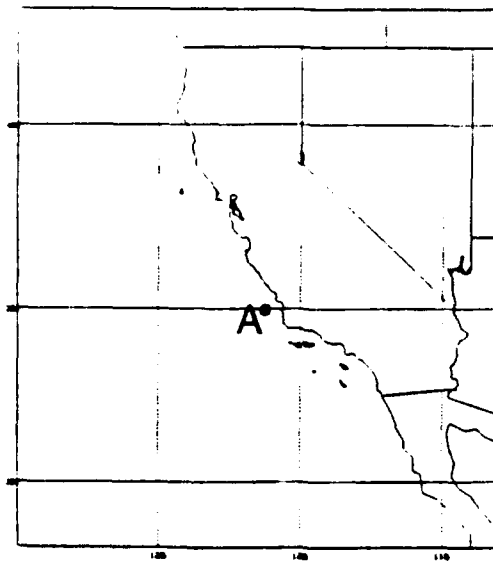


Figure 11
Control model time-height cross-section of
specific humidity (g/kg) at Point 'A'.

VI. TEST MODEL RUN EVALUATIONS

The test model, which utilizes the Sundqvist et al. explicit non-convective cloud water scheme, was compared with the control model. Stewart's (1992) incorporation of the Slingo and Ritter (1985) scheme into the NRL mesoscale model. Specific features compared were mesoscale wind structure, cloud fraction, longwave radiation, and temperature for the period 0000 UTC 02 May 1990 to 1200 UTC 03 May 1990. In addition, the depiction of cloud structure by cloud liquid water is evaluated and compared with that of cloud fraction. The evaluations focused on the cloud, temperature, radiation, and moisture structure within the boundary layer.

A. MESOSCALE WIND FEATURES-

Low-level wind fields defining the control model simulations of the Catalina eddy and southerly surge are described in Section V. Comparisons of test model to control model low-level winds revealed differences of less than 0.5 m/s between the fields. This may be explained by the incorporation of the cloud liquid water scheme predominantly affecting smaller scale features. The scheme also affects thermodynamic processes more than dynamic ones.

The Catalina eddy and southerly surge occur near the coastlines where the cloud cover test model simulations showed little change when compared to the control model.

Because of the similarities between these mesoscale wind fields, the following comparisons will focus on cloud fraction, temperature, and longwave radiation outputs.

B. CLOUD FRACTION-

Comparison of the control model to test model cloud fractions showed the test model to be more deficient than the control case in forecasting cloud cover over the region as verified against satellite observations. In fact the test model for 2100 UTC 02 May simulated no clouds at the 1000 mb level.

Since boundary layer depth has a direct effect on the relative humidity threshold values (RH_c) in the test model, the location of the boundary layer top appears to be the major reason for the test model's weakness in depicting cloud regions. Figure 12 illustrates the effects of a shallow versus a deep boundary layer on cloud formation. Because of the assumption of a linear decrease of RH_c with height to the top of the boundary layer, a shallow boundary layer results in lower RH_c values within the layer making it easier to produce clouds at those lower levels. On the

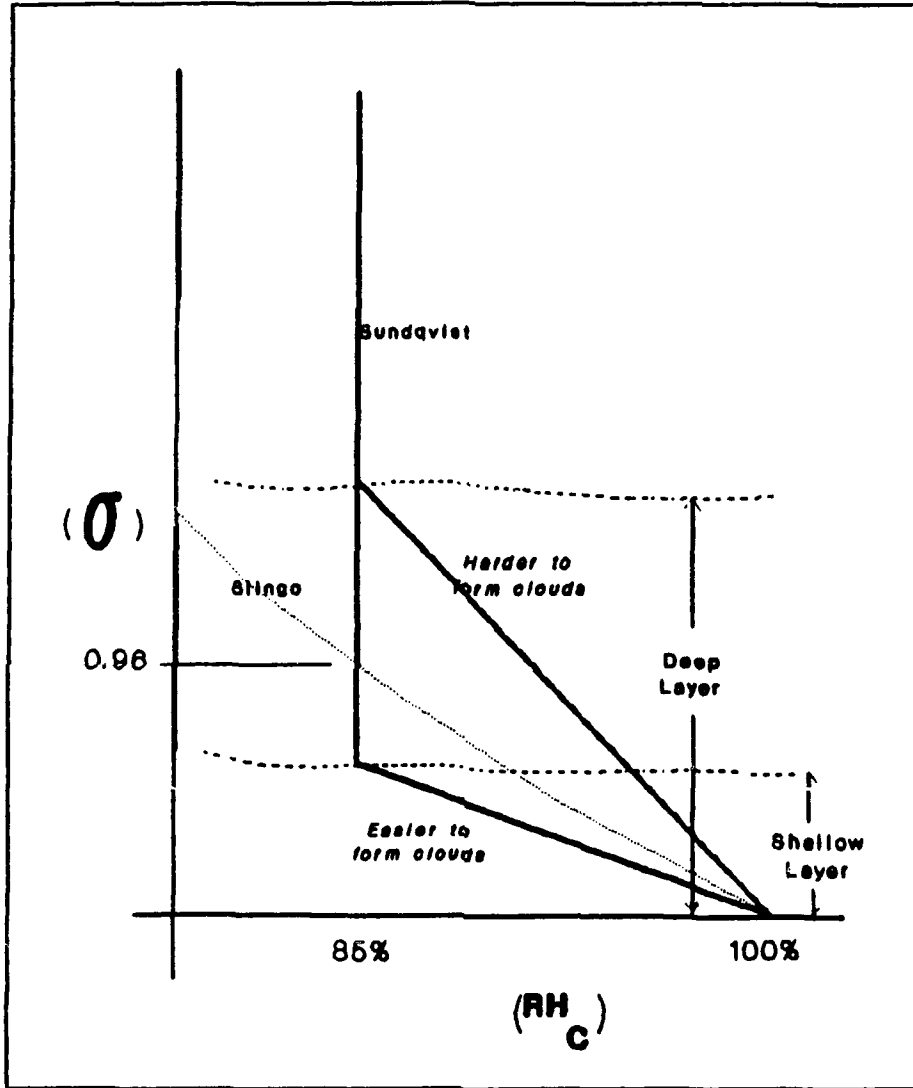


Figure 12

Effect of Boundary Layer Depth
on cloud formation.

other hand, a deep layer results in more difficulty producing clouds.

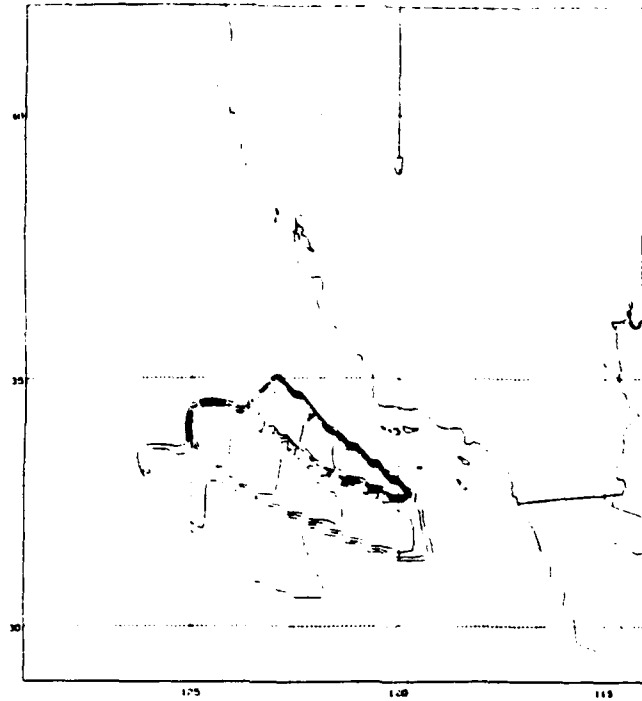
Also shown in Figure 12 is the height at which Slingo and Ritter's lower RH_c profile coincides with the Sundqvist et al. profile (over water). This occurs when the top of the boundary layer is at a sigma level of about 0.96. Therefore a boundary layer depth less than approximately 400 meters is required for the test model to produce clouds before the control model. Examination of boundary layer structure over the ocean for this case generally showed depths greater than 400 meters. Hence, one would not expect increased low-level cloud formation in the test model.

Stewart (1992) described the inability to diagnose certain cloudy regions as one of the weaknesses of the control model, resulting in his modification of the critical relative humidity profile at the low levels (the dashed line of Figure 4). Stewart's profile allows more cloud formation at the lower levels. Thus, henceforth the control model will be compared with two additional model runs -- one using the Sundqvist et al. explicit cloud liquid water scheme but retaining the Slingo critical relative humidity profile (test model 'A'), and one using the Sundqvist et al. scheme incorporating Stewart's proposed modified profile (test model 'B').

1. Cloud Fraction (Control Model vs Test Model 'A')-

Comparison of 1000 mb cloud fractions for 2100 UTC 02 May for this case (Figure 13) shows that test model 'A' significantly extended the cloud region westward and southward from approximately 32°N, 125°W. However, there was minimal effect toward the California coastline. The differences in the cloud fractions are due to differences in relative humidity. The inclusion of the Sundqvist et al. (1989) cloud liquid water scheme causes a temperature decrease in regions of cloud liquid water. The temperature drop in these regions consequently results in higher RH values. Temperature effects are discussed further in Part D of this Section.

Figure 14 compares RH values at 1000 mb. The increased relative humidities toward the southwest quadrant account for the increased cloud cover in that region. The coastal relative humidities on the other hand remain fairly constant resulting in minimal cloud cover increase near the coast.



2100 UTC 02 May 90 (Contour interval=0.1)

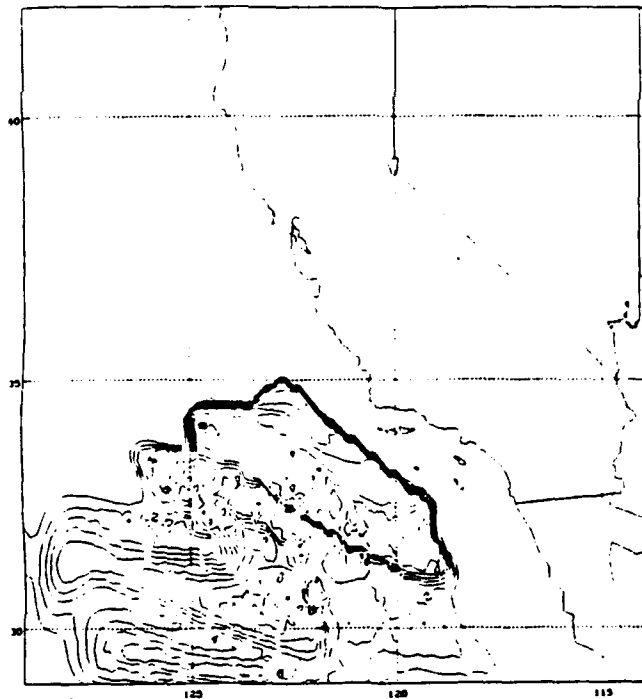


Figure 13
1000 mb cloud fraction.
Control model - top
Test model 'A' - bottom

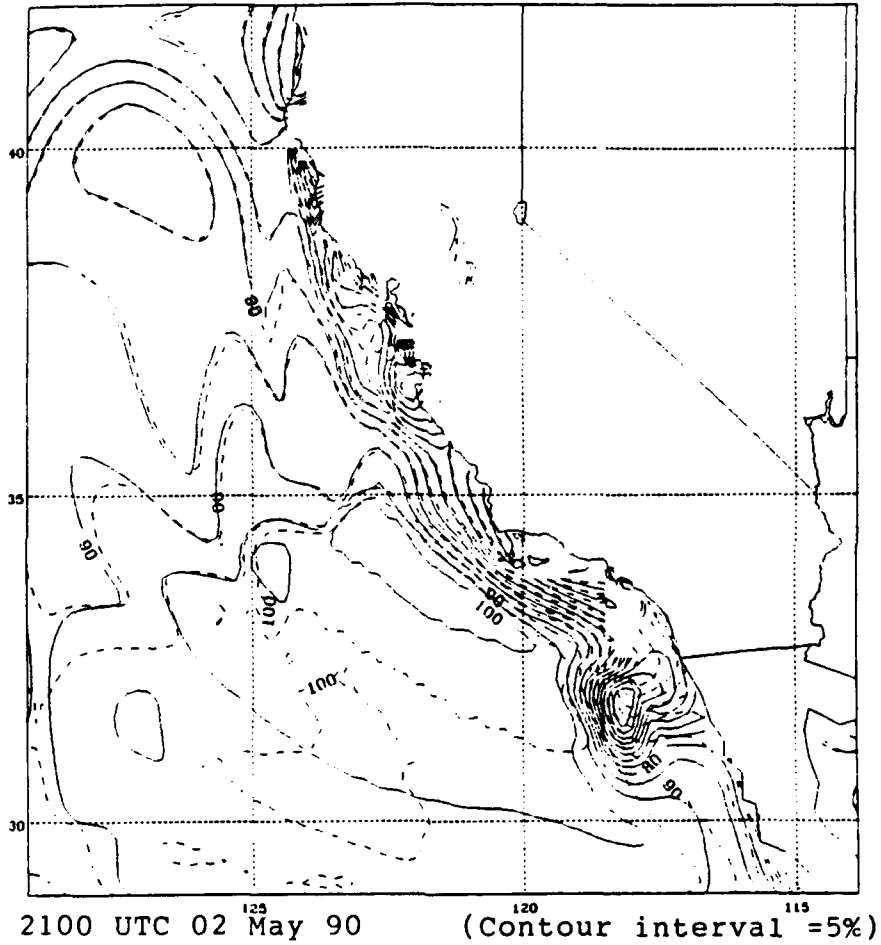


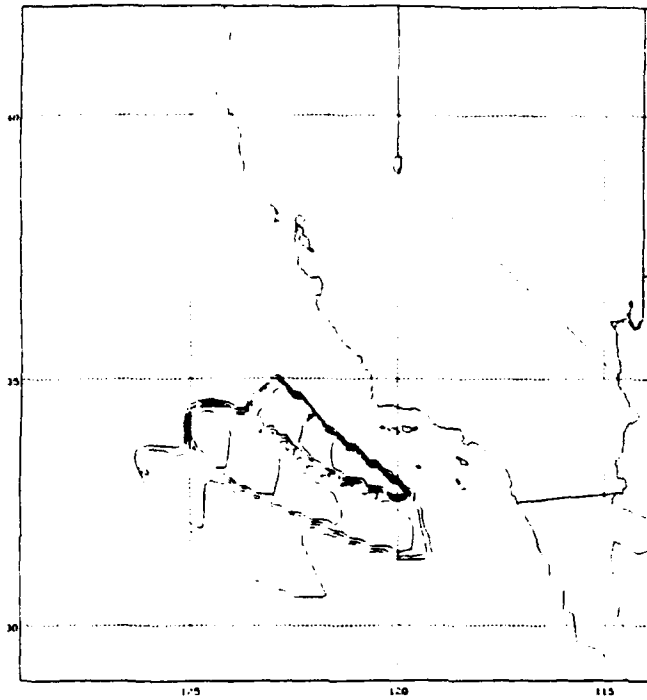
Figure 14
1000 mb relative humidity.
(control model -- solid)
(test model 'A' -- dashed)

2. Cloud Fractions (Control Model vs Test Model 'B')-

Test model 'B', in addition to extending the low-level cloud region westward similar to case 'A', also realistically extended the cloud region toward the California coast (Figure 15). Since Stewart modified RH_c values to help produce more model-simulated clouds by using satellite imagery and observations, this extension of clouds along the coastline can be expected.

Satellite imagery (2030 UTC visible image, Figure 9) showed a low-level tongue of coastal cloudiness from Monterey Bay to San Luis Obispo Bay that the model did not simulate. In addition, the model predicts low-level cloud cover out about 100 nm seaward from the coast ($34^\circ N$, $123^\circ W$) where generally clear skies were observed. The sea surface temperature (SST) fields used in these simulations were from 0000 UTC 02 May 1990 and kept constant throughout the time period. The constant SST fields may be part of the reason for the model cloud fraction weaknesses. SST values warmer than or approximately equal to the surface air temperature may result in more low-level clouds due to increased boundary layer flux convergence while significantly cooler model SST values could inhibit cloud formation.

As discussed in Section V, the control model's (and subsequently the test model's) simulation of low-level winds resulted in a much shorter duration southerly surge event as



2100 UTC 02 May 90 (Contour interval=0.1)

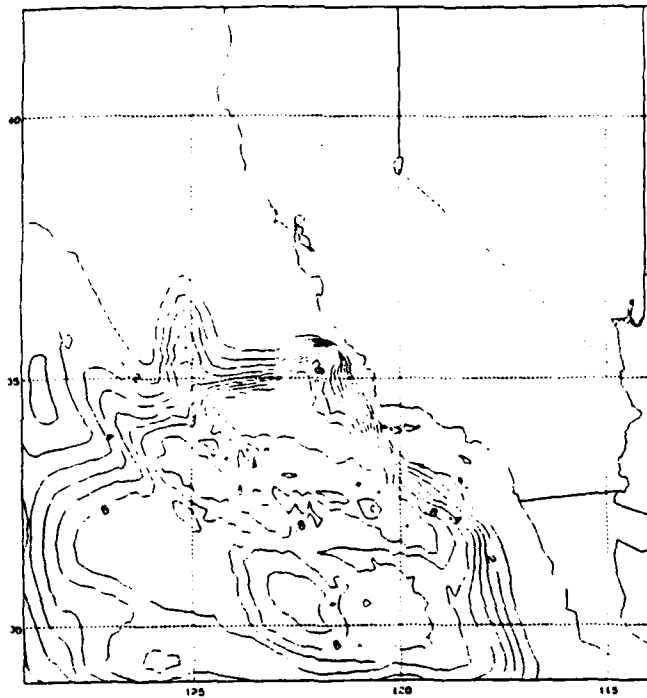


Figure 15
1000 mb cloud fraction.
Control model - top
Test model 'B' - bottom

compared with wind observations along the California coast. Since the southerly surge often produces persistent coastal cloudiness, the weaker model simulation of southerly winds may be another cause of the model's weakness in producing clouds up to the coastline.

The increased model-simulated cloud cover should affect the radiation and temperature fields at and below the cloud levels. This is evaluated in the following sections.

C. LONGWAVE RADIATION-

Figure 16 depicts an idealized longwave radiation profile in relation to a stratocumulus cloud (Stull 1988). A maximum longwave cooling rate is expected at the top of the cloud boundary with minimal cooling above the cloud. Also weaker longwave heating may be expected at the cloud base.

Longwave radiation along with cloud fraction and cloud liquid water profiles are shown in Figure 17 for Point 'B' (33° N, 122° W) for test model 'A' at 2100 UTC 02 May. Cloud tops occur at about 990 mb for both cloud fraction and cloud liquid water representations. Also, cloud fraction and cloud liquid water profiles depict the cloud base at about 1005 mb. Maximum longwave cooling of approximately 78°C/day occurs within the cloud at about 1000 mb with a heating rate of about 17°C/day at the cloud bottom. Evaluating this

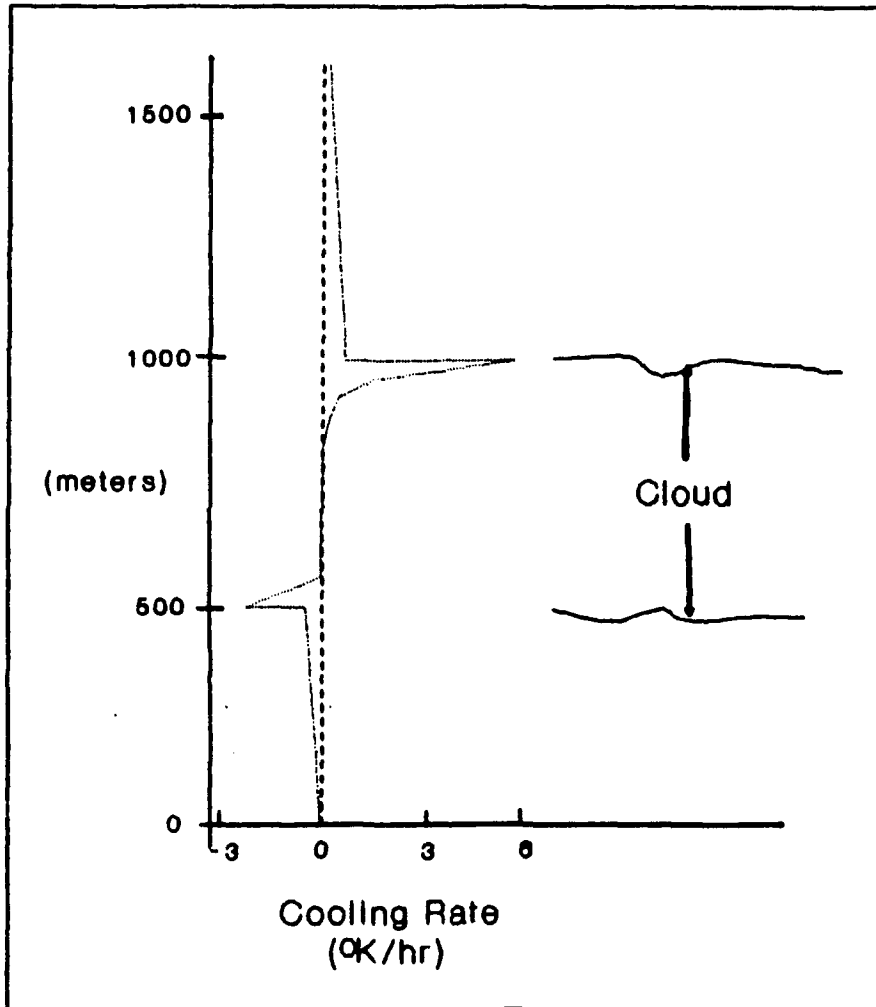


Figure 16
 Idealized longwave radiation cooling rate
 profile in a stratocumulus deck.
 (Stull 1988)

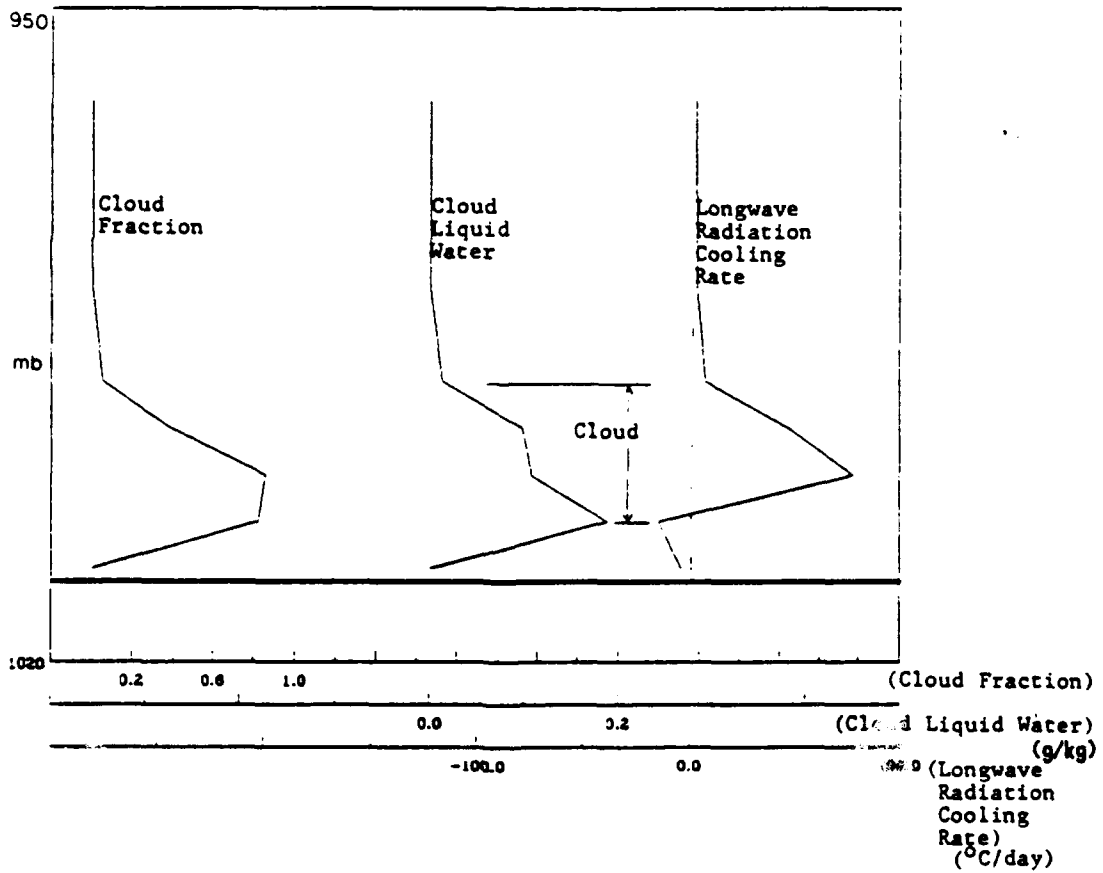
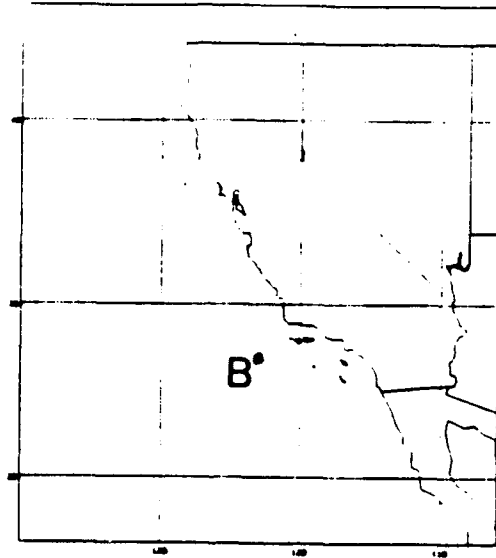


Figure 17
Longwave radiation cooling profile
at Point 'B'
(Test model 'A', 2100 UTC 02 May 90)

model radiation profile with the ideal case represented in Figure 16 shows that the model's maximum longwave radiative cooling is represented favorably though the model locates the cooling maximum at a lower level within the cloud. Incorporation of the cloud liquid water scheme provides direct interaction of the cloud with the environmental temperature and moisture profiles. This interaction is evident in the equations (3.1, 3.6, and 3.7) as given by Sundqvist. Thus changes in cloud liquid water as computed at every gridpoint and for each iteration in the model directly impact the temperature and moisture of the atmosphere.

However, these changes in cloud liquid water are not as readily apparent when comparing cloud liquid water to cloud fraction. This is because cloud fraction is computed along with radiation parameters every half hour (60 iterations). Thus the indirect effect of cloud liquid water on cloud fraction through changes in temperature and moisture profiles is not readily visible in comparisons. Hence, cloud liquid water provides a more physically realistic determination of cloud structure and subsequent radiation profiles, though for comparisons of model simulations there is a more direct, one-to-one relationship between cloud fraction and radiation than cloud liquid water and radiation.

D. TEMPERATURE-

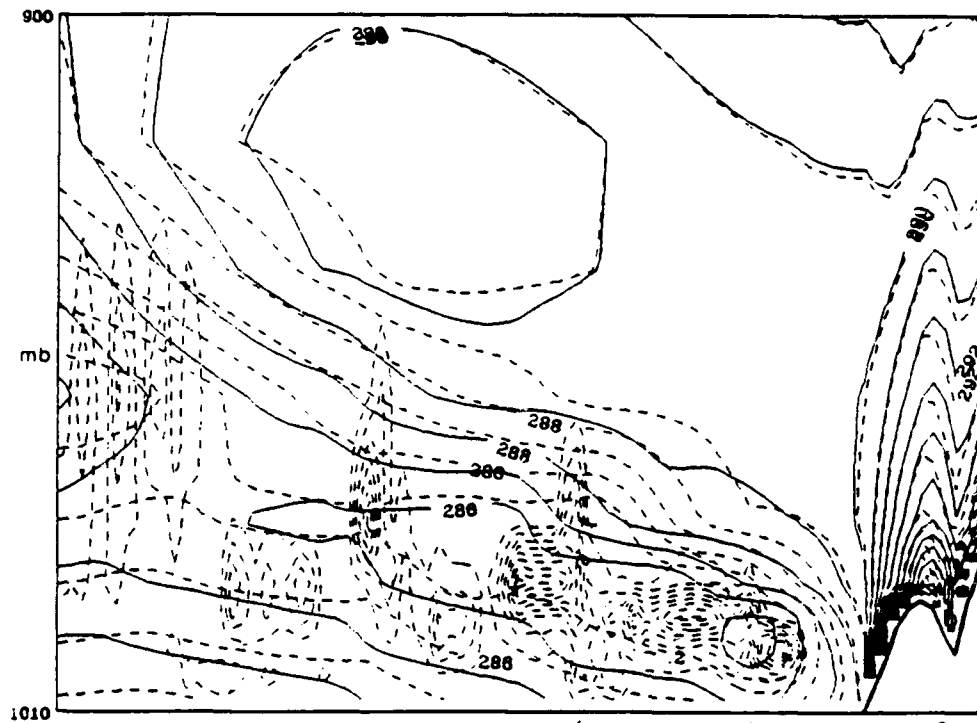
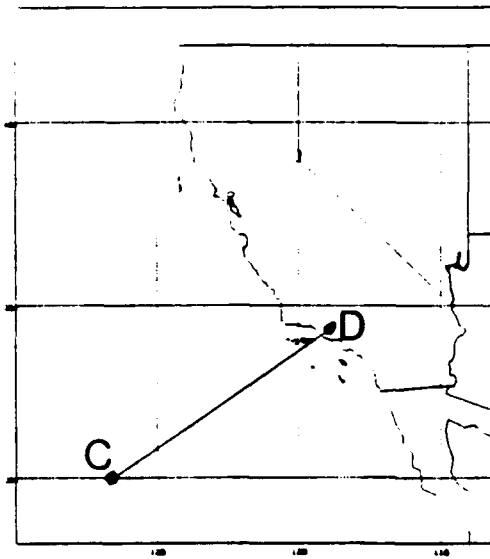
Temperature field comparisons revealed significant differences between the control model and test models 'A' and 'B'. The temperature differences occurred within the model-simulated cloud regions for both test models.

1. Temperature (Control Model vs Test Model 'A')-

Figure 18 shows low-level cross-section temperature comparisons of the control model and test model 'A' for a predominantly cloud-covered region from Point 'C' to 'D' at 2100 UTC 02 May. Temperatures were as much as 2°C lower for test model 'A' versus the control model in areas within and below the dense clouds. Figure 19 for Point 'B' shows that temperature deviations occurred from the surface up to about 960 mb with the maximum difference occurring within the cloud boundaries.

2. Temperature (Control Model vs Test Model 'B')-

Low-level cross-section temperature comparison for the same region described above is shown in Figure 20. Similar to test model 'A', temperatures in test model 'B' were lower by as much as 4°C within cloud regions as compared to the control model. The temperature field



(Contour interval=1°K)

Figure 18
Temperature cross-section from Point 'C' to 'D'
(2100 UTC 02 May 90)
Control model - solid
Test model 'A' - dashed

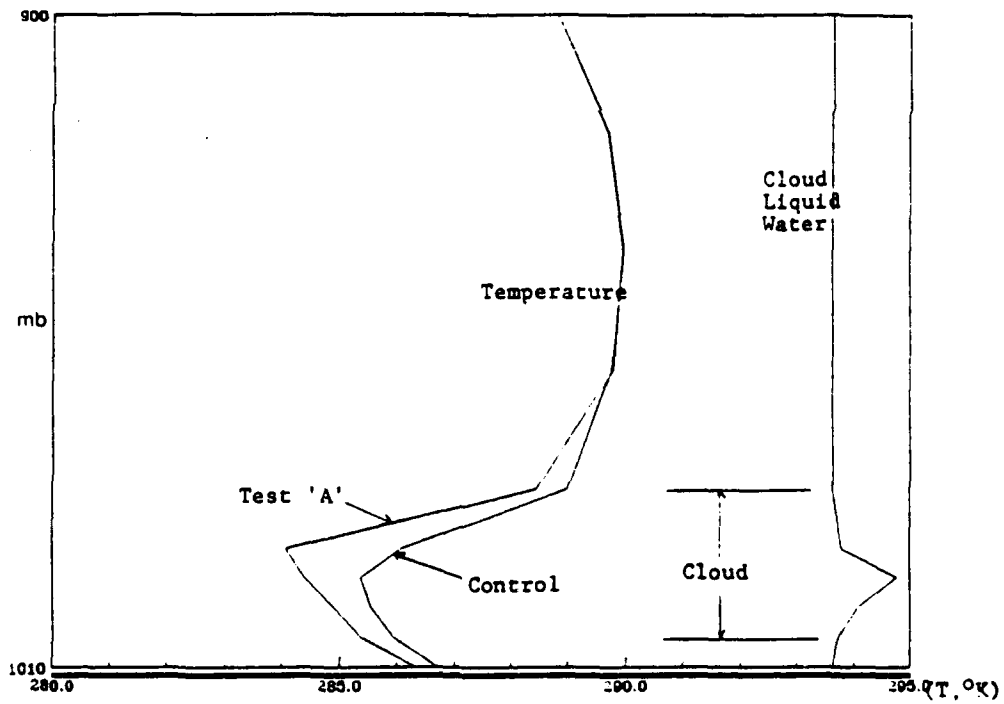
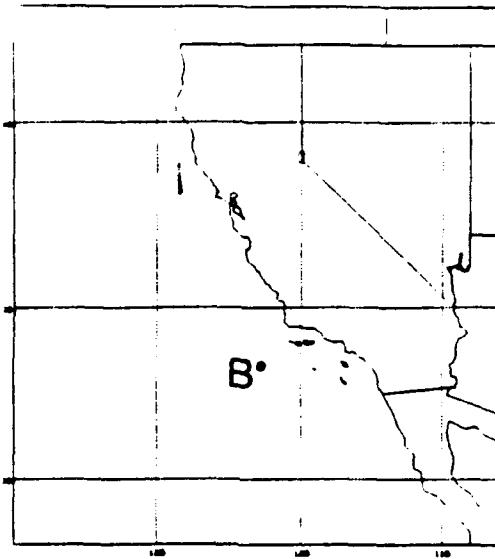


Figure 19
Temperature profile at Point 'B'
(2100 UTC 02 May 90)

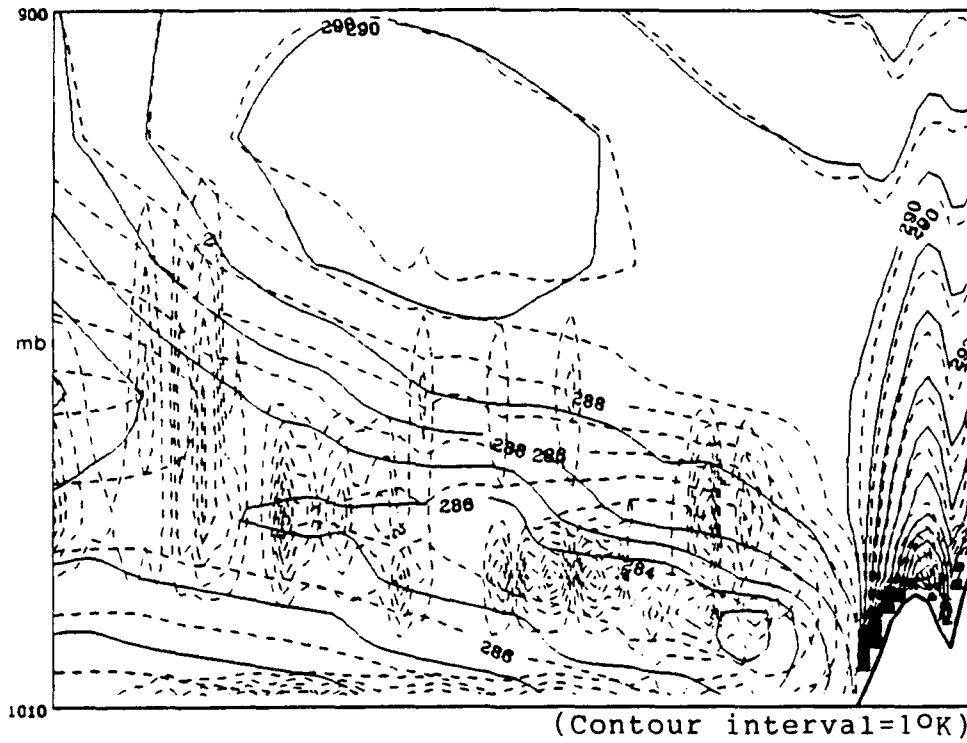
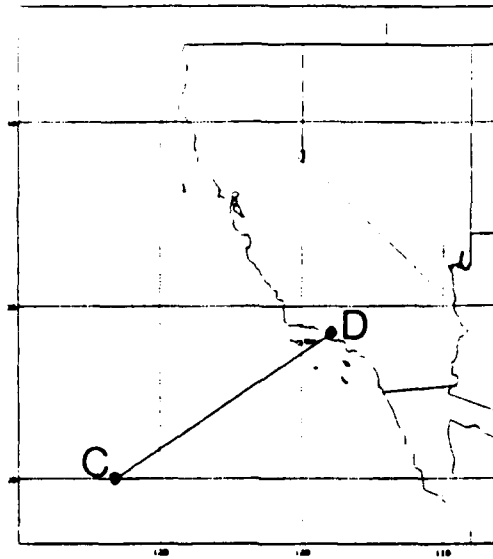


Figure 20
Temperature cross-section from Point 'C' to 'D'
(2100 UTC 02 May 90)
Control model - solid
Test model 'B' - dashed

difference for this case appeared to be larger due to thicker cloud depictions by the model.

Also comparable to test model 'A', Figure 21 for Point 'B' shows temperature profile deviation occurring within the same cloud boundary levels.

E. CLOUD LIQUID WATER-

Generally, low-level cloud liquid water regions closely follow the cloud fraction regions as seen in Figure 22. Note the rather smooth nature of cloud fraction (as dependent on RH) in contrast to the somewhat noisy structure of cloud liquid water.

An area of interest due to the lack of clouds at 1000 mb is located in the region's southwest quadrant (Figure 23). A comparison between the test model run 'B' 1000 mb cloud fraction and cloud liquid water fields for 2100 UTC 02 May show little or no cloud liquid water in that quadrant at 1000 mb. A cross section from point 'C' to 'D' (Figure 24) shows cloud liquid water generally throughout that region with relatively dry regions at the 1000 mb level. This layered cloud structure is often observed in the marine boundary layer. Use of the explicit cloud liquid water scheme allows for a realistic depiction of this layered structure that a simple cloud fraction scheme could not simulate. Note how the cloud liquid water cross section

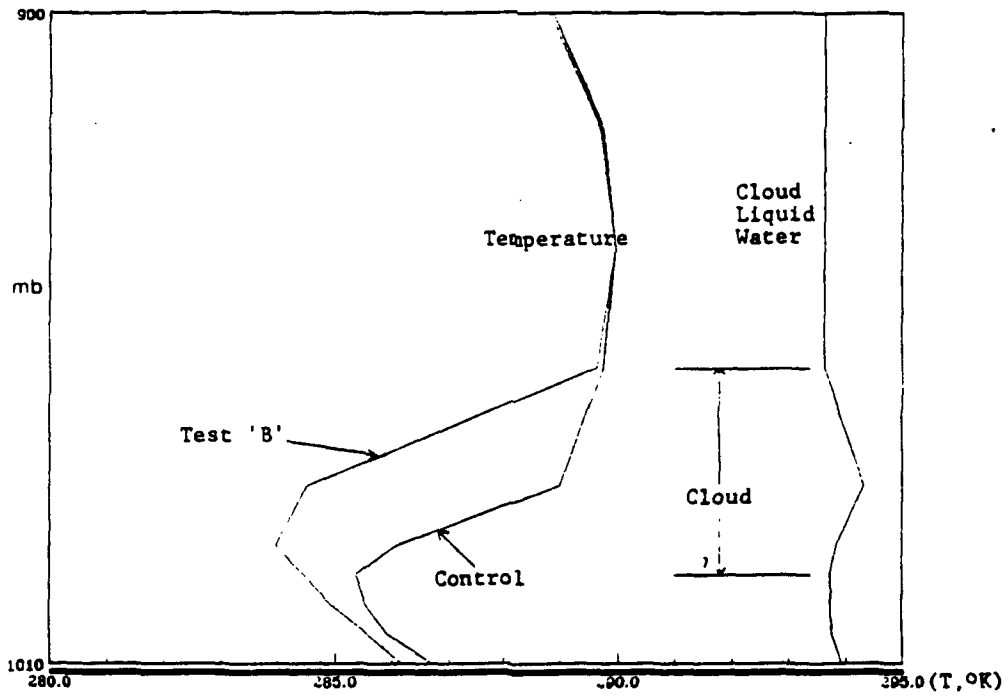
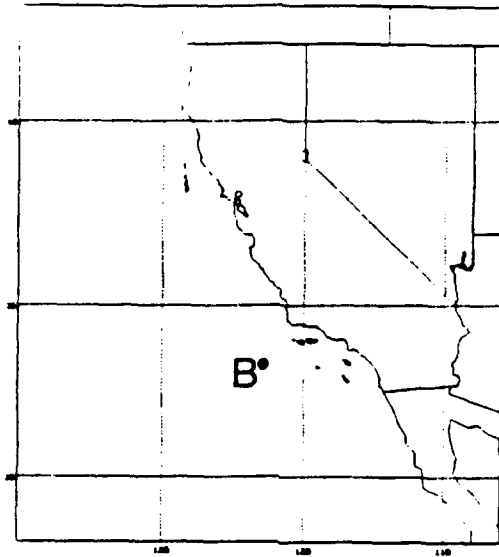
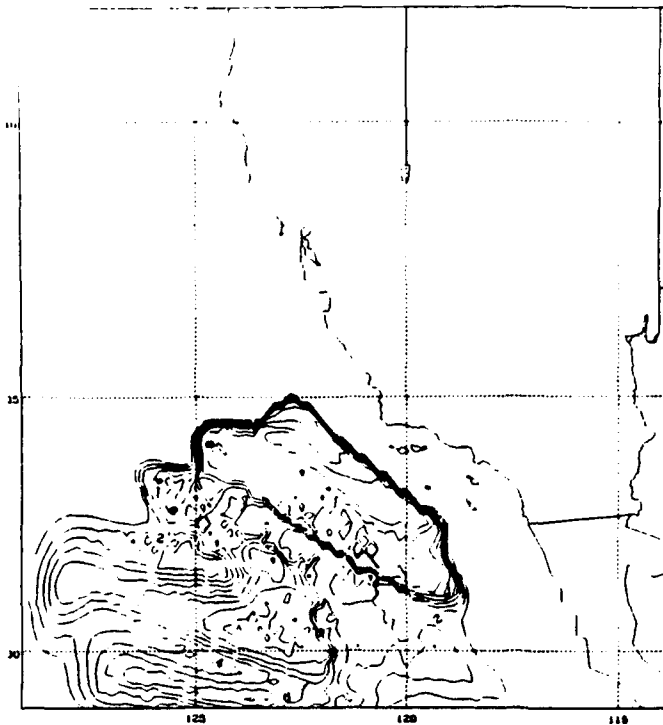
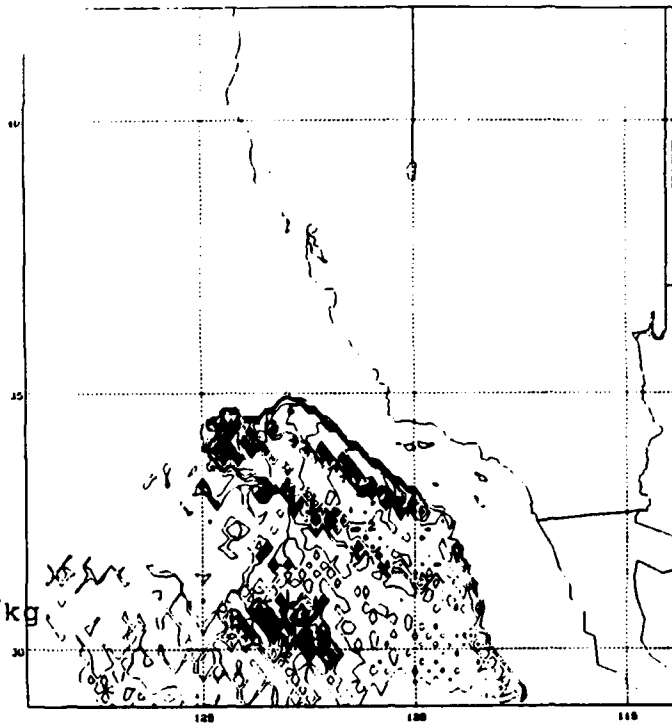


Figure 21
Temperature profile at Point 'B'
(2100 UTC 02 May 90)



Cloud Fraction
contour interval=0.1

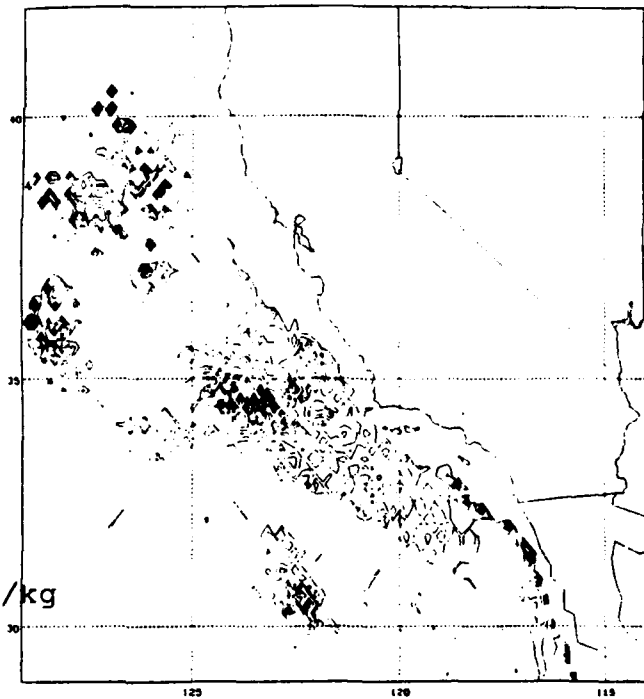


Cloud Liquid Water
contour interval=0.1 g/kg

Figure 22
 1000 mb cloud fraction (top)
 1000 mb cloud liquid water (bottom)
 (Test model 'A', 2100 UTC 02 May 90)



Cloud Fraction
contour interval=0.1



Cloud Liquid Water
contour interval=0.1 g/kg

Figure 23
1000 mb cloud fraction (top)
1000 mb cloud liquid water (bottom)
(Test model 'B', 2100 UTC 02 May 90)

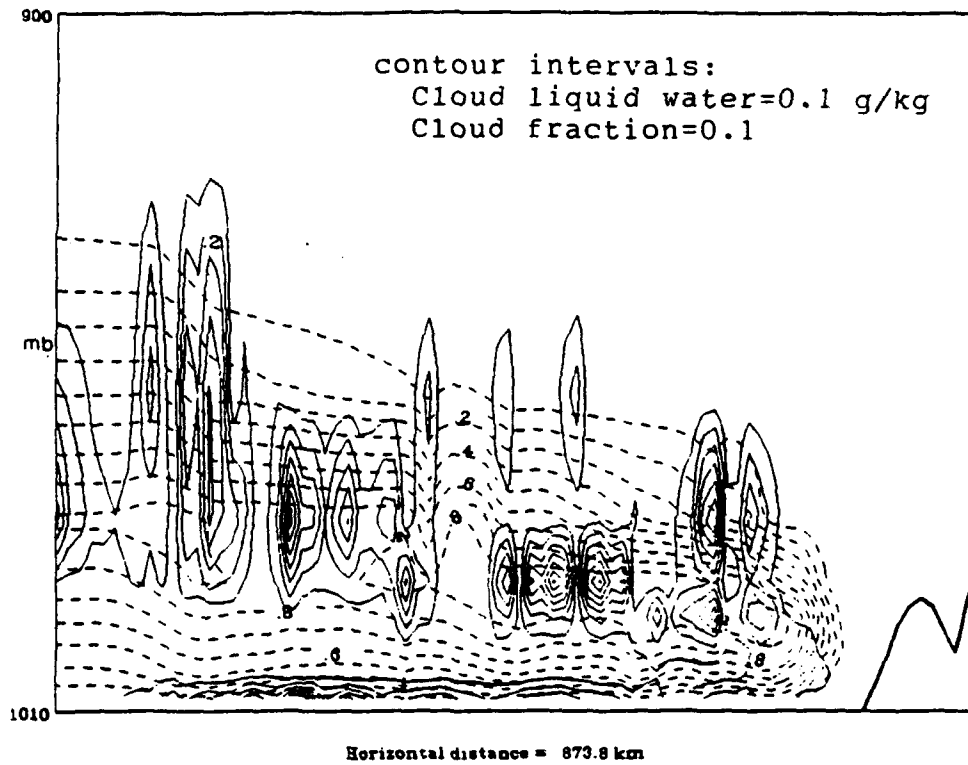
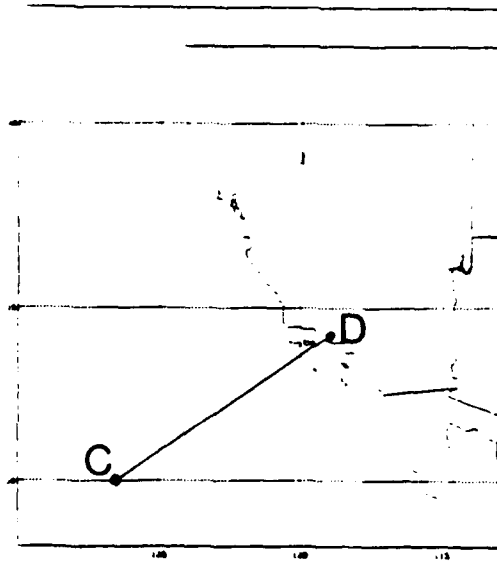


Figure 24
 Cloud liquid water (solid) and
 cloud fraction (dashed) cross-sections
 from Point 'C' to 'D'.
 (Test model 'B', 2100 UTC 02 May 90)

also provides a more realistic horizontal and vertical cloud texture appearance than the cloud fraction contours as compared in Figure 24. The cloud fraction is simply a representation of RH while cloud liquid water includes more of the physics needed in defining clouds and the boundary layer.

VII. CONCLUSIONS AND RECOMMENDATIONS

A. CONCLUSIONS-

This study has demonstrated that the incorporation of the Sundqvist et al. (1989) explicit non-convective cloud liquid water scheme into the NRL mesoscale model provides improvements in simulating longwave radiation, temperature, and cloud structure features over the U.S. West Coast Pacific region.

One limitation that was found in the incorporation of the Sundqvist scheme for this particular case was its extreme weakness in accurately diagnosing low-level clouds. The main reason for this weakness was Sundqvist's representation of relative humidity threshold values for cloud formation. Test model evaluations were therefore conducted using Sundqvist's cloud liquid water scheme but retaining Slingo's critical relative humidity profile for cloud formation (test model 'A'). In addition, test model 'B', which used a modified critical relative humidity profile by Stewart (1992) was also evaluated. This modified profile was proposed to help compensate for the control model's weakness in diagnosing low-level clouds over certain areas in the region. Test models 'A' and 'B' were able to provide a closer cloud cover picture of the region as

compared to satellite imagery, with test model 'B' showing more realistic cloud cover near the coast.

Longwave radiation profiles in cloud regions showed realistic and consistent cooling and warming rates as compared to idealized radiation profiles. Temperature effects due to model-simulated cloud cover also compared favorably.

A significant improvement in the NRL model was the realistic horizontal and vertical cloud structure that was represented by the cloud liquid water fields. Control model cloud depiction was only through cloud fraction, a representation of relative humidity. The introduction of cloud liquid water as a prognostic variable takes into account more of the physics involved in better defining cloud structure and the marine boundary layer. Cloud liquid water used as a portrayal of cloud cover provides a more physically realistic texture and layered structure associated with non-convective clouds.

B. RECOMMENDATIONS-

Stewart's (1992) study provided a modified RH_c profile to help provide a closer cloud depiction as compared to satellite imagery. Using this modified profile, better cloud cover representation was achieved but continued fine-tuning of the RH_c values for a variety of cases of differing synoptic flow may be necessary for a more accurate model cloud cover picture. An experiment utilizing a good dispersal of surface, ship, and buoy station observations with soundings along with satellite observations could provide a closer real world RH_c profile depiction.

Section VI described a situation where the 1000 mb cloud liquid water depiction showed very little or no clouds while satellite imagery clearly indicated low-level cloud cover over the area. A cross-section view of the test model cloud liquid water fields revealed a layered cloud structure with a dry area at the 1000 mb level. Development of a three-dimensional display capability would help provide an easier way of visualizing a complex cloud structure from cloud liquid water. Computation of cloud fraction at every iteration to correspond to cloud liquid water fields would aid in visual interpretation of clouds. In addition, other fields in the model may be easier visualized three-dimensionally.

This study incorporated the Sundqvist et al. (1989) non-convective cloud scheme into the NRL model but did not include Sundqvist's scheme for convective clouds. Further study incorporating the convective cloud scheme is recommended as a follow on.

Finally, an evaluation of the realistic cloud structure by cloud liquid water in regions of available data could verify the accuracy of the cloud portrayals and provide a better degree of confidence in the overall model outputs.

REFERENCES

- Bosart, L.F., 1983: "Analysis of a California Eddy Event," Mon. Wea. Rev., **111**, 1619-1633.
- Chang, S.W., 1979: "An Efficient Parameterization of Convective and Non-Convective Planetary Boundary Layers for Use in Numerical Models," J. Appl. Meteor., **18**, 1205-1215.
- Chen, C., and W.R. Cotton, 1987: "The Physics of the Marine Stratocumulus-capped Mixed Layer," J. Atmos. Sci., **44**, 2951-2977.
- Corkill, P.W., 1991: Synoptic and Mesoscale Factors Influencing Stratus and Fog in the Central California Coastal Region, Master's Thesis, Meteorology Department, Naval Postgraduate School, Monterey, California.
- Dorman, C.E., 1985: "Evidence of Kelvin Waves in California's Marine Layer and Related Eddy Generation," Mon. Wea. Rev., **113**, 827-839.
- Grandau, F.J., 1992: Evaluation of the Naval Research Laboratory Limited Area Dynamical Weather Prediction Model: Topographic and Coastal Influences Along the West Coast of the United States, Master's Thesis, Meteorology Department, Naval Postgraduate School, Monterey, California.
- Harshvardhan, R. Davies, D.A. Randall, and T.G. Corsetti, 1987: "A fast Radiation Parameterization for Atmospheric Circulation Models," J. Geophys. Res., **92**, 1009-1016.
- Holt, T., and S. Raman, 1988: "A Review and Comparative Evaluation of Multi-level Boundary Layer Parameterizations for First Order and Turbulent Kinetic Energy Closure Schemes," Rev. Geophys., **26**, 761-780.
- Kuo, H.L., 1974: "Further Studies of the Parameterization of the Influence of Cumulus Convection on Large Scale Flow," J. Atmos. Sci., **31**, 1232-1240.

- Madala, R.V., S.W. Chang, U.C. Moharty, S.C. Madan, R.K. Paliwal, V.B. Sarin, T. Holt, and S. Raman, 1987: Description of the Naval Research Laboratory Limited Area Dynamical Weather Prediction Model, NRL Technical Report 5992.
- Mass, C.F., and M.D. Albright, 1989: "Origin of the Catalina Eddy," Mon. Wea. Rev., **117**, 2406-2436.
- Slingo, J.M., and B. Ritter, 1985: "Cloud Prediction in the ECMWF Model," ECMWF Tec. Rep. No. 46, 48 pp.
- Stewart, P.C., 1992: Incorporation of a Radiation Parameterization Scheme into the Naval Research Laboratory Limited Area Dynamical Weather Prediction Model, Master's Thesis, Meteorology Department, Naval Postgraduate School, Monterey, California.
- Stull, R.B., 1988: An Introduction to Boundary Layer Meteorology, Kluwer Academic Publishers.
- Sundqvist, H., 1988: "Parameterization of Condensation and Associated Clouds in Models for Weather Prediction and General Circulation Simulation," Physically-Based Modelling and Simulation of Climate and Climatic Change, M.E. Schlesinger, Ed., Reidel, 433-461.
- Sundqvist, H., E. Berge, and J.E. Kristjansson, 1989: "Condensation and Cloud Parameterization Studies with a Mesoscale Numerical Weather Prediction Model," Mon. Wea. Rev., **117**, 1641-1657.

INITIAL DISTRIBUTION LIST

	No. Copies
1. Defense Technical Information Center Cameron Station Alexandria, VA 22304-6145	2
2. Library, Code 52 Naval Postgraduate School Monterey, CA 93943-5002	2
3. Chairman (Code MR/Hy) Department of Meteorology Naval Postgraduate School Monterey, CA 93943-5000	1
4. Chairman (Code OC/Co) Department of Oceanography Naval Postgraduate School Monterey, CA 93943-5000	1
5. Professor Teddy R. Holt (Code MR/Ht) Department of Meteorology Naval Postgraduate School Monterey, CA 93943-5000	1
6. Professor Philip A. Durkee (Code MR/De) Department of Meteorology Naval Postgraduate School Monterey, CA 93943-5000	1
7. Dr. Simon Chang Naval Research Laboratory Code 7220 Washington, D.C. 20375	1
8. Dr. John Hovermale Naval Research Laboratory-Monterey Monterey, CA 93943-5006	1
9. Dr. Lee Eddington Geophysics Division Pacific Missile Test Center Point Mugu, CA 93042-5000	1

10. Dr. Gary Geernaert 1
Office of Naval Research
Code 1122MM
800 N. Quincy St.
Arlington, VA 22217-5000
11. LCDR Damacene V. Ferandez 1
Naval Oceanography Command Detachment
PSC 486, Box 1243
FPO, AP 96506-1243